

Feedback loops are central to the dynamics of mental disorder symptoms

Received: 5 September 2025

Accepted: 30 January 2026

Published online: 20 February 2026

Cite this article as: Park K., Li X., Waldorp L. *et al.* Feedback loops are central to the dynamics of mental disorder symptoms. *Sci Rep* (2026). <https://doi.org/10.1038/s41598-026-38747-6>

Kyuri Park, Xinhai Li, Lourens Waldorp, Mike Lees & Vitor V. Vasconcelos

We are providing an unedited version of this manuscript to give early access to its findings. Before final publication, the manuscript will undergo further editing. Please note there may be errors present which affect the content, and all legal disclaimers apply.

If this paper is publishing under a Transparent Peer Review model then Peer Review reports will publish with the final article.

ARTICLE IN PRESS

The Role of Feedback Loops in Dynamical Symptom Networks

Kyuri Park^{*1}, Xinhai Li², Lourens Waldorp^{3,4}, Mike Lees^{1,4,5}, and Vítor V. Vasconcelos^{1,4,5}

¹*Computational Science Lab, Informatics Institute, University of Amsterdam, PO Box 94323, Amsterdam, 1090GH, The Netherlands*

²*Graduate School of Informatics, University of Amsterdam, PO Box 94323, Amsterdam, 1090GH, The Netherlands*

³*Department of Psychology, University of Amsterdam, Nieuwe Achtergracht 129, Amsterdam, 1018WT, The Netherlands*

⁴*Institute for Advanced Study, University of Amsterdam, Oude Turfmarkt 147, Amsterdam, 1012GC*

⁵*Centre for Urban Mental Health, University of Amsterdam, Amsterdam, The Netherlands*

Author Note

Kyuri Park  <https://orcid.org/0000-0001-8502-2134>

Correspondence concerning this article should be addressed to Kyuri Park, Computational Science Lab, Informatics Institute, University of Amsterdam, PO Box 94323, Amsterdam, 1090 GH, the Netherlands. E-mail: k.park@uva.nl.

FEEDBACK LOOPS IN SYMPTOM NETWORKS

Abstract

Feedback loops are central to the dynamics of mental disorder symptoms, serving as mechanisms that sustain and amplify symptoms over time. Despite their importance, the influence of feedback loop structures on symptom progression and persistence remains underexplored. Here, we introduce a general simulation-based framework for analyzing feedback-loop architecture in dynamical symptom networks and demonstrate it using a 9-node depression symptom network based on the PHQ-9. This study bridges this gap by analyzing a family of simulation models of symptom dynamics describing 98,304 directed networks compatible with empirically observed correlation symptom networks and their feedback loops. Systematic simulations of diverse network configurations revealed that while increasing the number of feedback loops elevates symptom levels, this effect plateaus due to the diminishing impact of overlapping loops. Additionally, networks with evenly distributed connectivity sustain higher symptom levels, necessitating the disruption of multiple feedback loops simultaneously to weaken the network's cohesive structure and reduce symptom persistence. Empirical alignment using real-world clinical data supports these findings, demonstrating that frequently observed edges in network structures align with simulated configurations that drive high symptom levels. These results demonstrate that symptom severity and persistence are determined not merely by the presence of feedback loops but by their specific connections. These findings motivate intervention strategies that prioritize disrupting influential feedback structures and key connections rather than broadly reducing connectivity. By integrating computational modeling and empirical analysis, this study advances our understanding of symptom persistence and offers insights for designing targeted interventions to mitigate symptom severity and relapse risk.

Keywords: Feedback loops, dynamical system, computational model, symptom network, mental health

FEEDBACK LOOPS IN SYMPTOM NETWORKS

The Role of Feedback Loops in Dynamical Symptom Networks

The network approach to understanding mental disorders has introduced a new way of thinking about the dynamics of symptoms. Instead of viewing symptoms in isolation, this approach considers them to be part of a connected system where each symptom can influence others [1]. This perspective has spurred extensive research into the structure and function of these networks, emphasizing how interactions between symptoms could contribute to the persistence and severity of mental health conditions [2–7]. A prominent theme within this literature is the role of feedback loops — cyclic relationships where symptoms reinforce each other. Such loops are thought to make disorders difficult to treat by sustaining and amplifying activation over time [8–11]. For instance, in depression, symptoms like sleep problems and sadness are often thought to reinforce each other — sleep issues can lead to feeling down, which in turn results in sleepless nights filled with worrying thoughts — creating a feedback loop that makes recovery more challenging [12].

Although the importance of cyclic dynamics is widely acknowledged, most accounts remain qualitative about what loop structures actually do [9, 13]. In depression, reinforcing (“vicious cycle”) mechanisms are frequently discussed [8–11], yet direct empirical identification of specific symptom-level directed feedback cycles remains challenging in practice and is therefore less developed than theoretical and hypothesis-driven accounts.

Prior work has emphasized their theoretical impact—e.g., persistence via hysteresis [14]—but offers limited guidance on which loop configurations matter most, or how their arrangement shapes trajectories [8, 9, 13]. Recent advances on the resilience side of the literature help at the macro level: Lunansky et al. [15] formalize a complex-systems framework in which symptom networks fall within a “resilience quadrant” (healthy–dysfunctional; stable–unstable) based on simulated responses to perturbations. What remains unclear, and is the focus here, is the micro-architecture of feedback: how the number of loops, their overlap, and the distribution of connectivity across nodes jointly govern persistence and severity.

Our contribution is to move beyond the general claim that “feedback loops matter” by

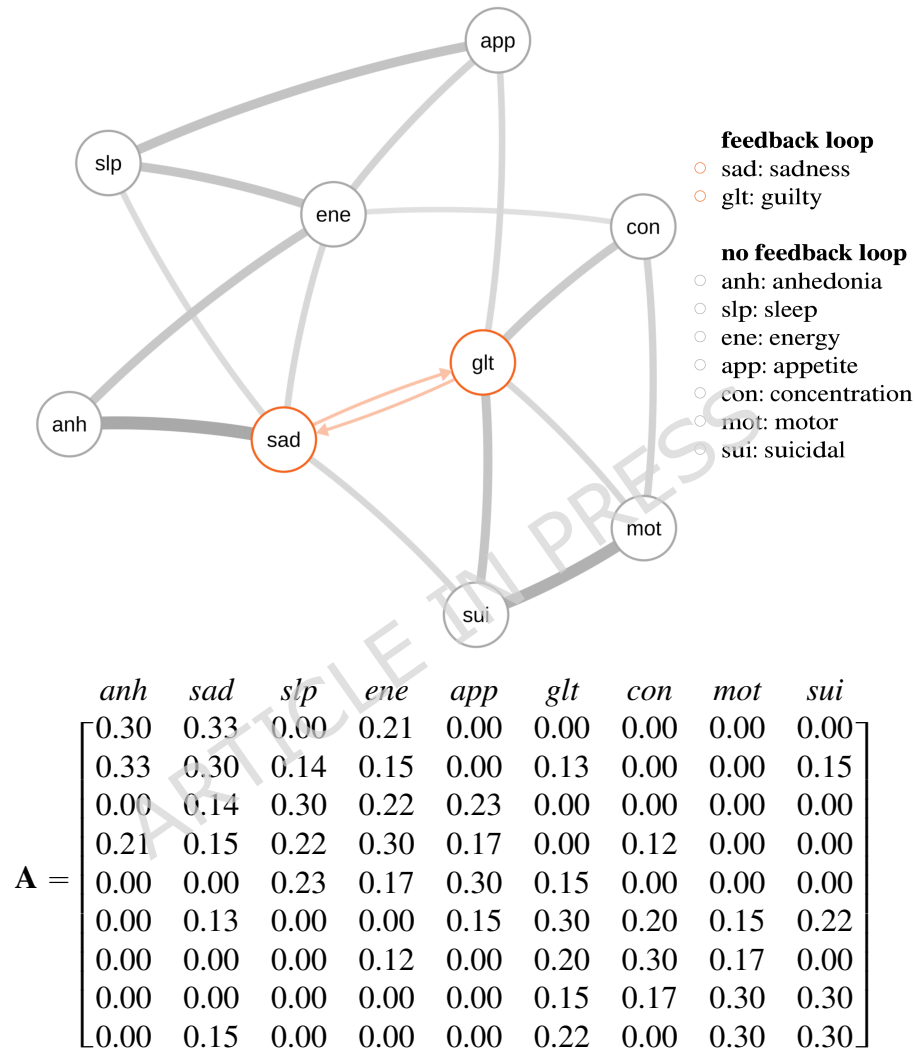
FEEDBACK LOOPS IN SYMPTOM NETWORKS

systematically testing which feedback-loop *architectures* matter and how they shape post-shock trajectories. Specifically, we examine (i) how many reinforcing cycles exist, (ii) how much they overlap by sharing nodes, and (iii) how evenly connectivity is distributed across symptoms. This loop-architecture perspective complements classical network summaries (e.g., density or centrality) by characterizing how reinforcing pathways are arranged and interdependent, not merely how connected the network is.

We present a general framework applicable to symptom networks across psychopathology; we demonstrate and evaluate it using a single worked example: a nine-symptom depression network based on the PHQ-9 (Figure 1). We adopt an empirically informed reference network introduced in prior work [16–19] and use it as a starting point for systematically exploring directed configurations and feedback structures; methodological details on how the reference network was specified and parameterized are provided in the [Methods](#). The simulation results reported below refer to directed configurations of this PHQ-9 network, but the results hold also for different networks; we used the PHQ-9 network as a generic example.

Using the depressive-symptom dynamics model of Park, Waldorp, and Vasconcelos [16], we systematically vary network *structure* while holding other elements constant. Starting from an empirically informed, correlation-based *undirected* symptom skeleton [16], we enumerate all feasible *directed* orientations (including cycles) consistent with that scaffold, treating the resulting ensemble as candidate causal graphs grounded in observed associations—an approach aligned with using statistical networks as structural scaffolds for simulation-based causal exploration [20, 21]. We further extend this analysis to other network topologies that do not derive from the data to show the robustness and generality of our results. For each orientation, we simulate trajectories following a transient perturbation and summarize post-shock symptom levels at multiple time points, relating persistence to three topological features: the *number of feedback loops*, the *degree of loop overlap* (shared nodes among loops), and *weighted degree variability* across nodes (σ_{tot}), indexing how evenly connectivity is distributed. We include σ_{tot} because networks with similar loop structure can nonetheless differ in whether influence is broadly distributed or concentrated in

FEEDBACK LOOPS IN SYMPTOM NETWORKS

**Figure 1**

Reference network skeleton of depressive symptoms with one dyadic feedback loop and its weighted adjacency matrix \mathbf{A} . Self-loops α_{ii} (diagonal elements of \mathbf{A}) are omitted in the network visualization for readability; they are implemented as within-symptom self-effects in the dynamics but are not counted as feedback loops in our loop-architecture analyses.

FEEDBACK LOOPS IN SYMPTOM NETWORKS

a few symptoms. To identify concrete targets, we contrast node- and edge-level loop participation between networks that sustain high versus low symptom levels. We then assess external consistency by estimating directed networks from an independent clinical time-series dataset using PCMCI+ (PC Momentary Conditional Independence), a causal discovery method for time-series data [22–24], and by comparing their most frequent edges with those characterizing high-symptom simulations. We discuss how these simulation-derived patterns align with real-world observations and what they could imply for targeting symptom dynamics. Motivated by evidence that some individuals remain in prolonged high-symptom states [25, 26], we show (i) when adding loops increases persistence and when effects saturate, (ii) how overlap and connectivity balance modulate these effects, and (iii) which edges/loops are consistently associated with sustained high symptoms.

Results

We examine symptom persistence as a function of the abundance and organization of feedback loops, namely loop count, loop overlap, and connectivity balance, and relate them to post-shock symptom levels. We then analyze loop micro-architecture at the node and edge levels to identify structural motifs associated with high symptom prevalence. These motifs are interpreted as simulation-derived, hypothesis-generating patterns (formalizing "vicious cycle" intuitions), rather than as direct empirical confirmation of symptom-level causal cycles. Finally, we assess external consistency by comparing simulation-derived motifs to directed edges estimated from patient time-series networks using PCMCI+ (see Section [Methods](#) for details).

Overall Network Structure Analysis

Figure 2 illustrates the relationship between the number of feedback loops in networks and their corresponding aggregated symptom levels. The x-axis groups networks by the number of feedback loops, while the y-axis shows the aggregated symptom levels, averaged across 50 iterations. Each color represents a specific time point — $t = 400$ (teal), $t = 800$ (yellow), $t = 1200$ (red), $t = 1600$ (green), and $t = 2000$ (purple) — with boxplots displaying the

FEEDBACK LOOPS IN SYMPTOM NETWORKS

distribution of the symptom levels at each time point. Here, simulation time point t is an abstract model time index and is not calibrated to a specific real-world unit. We interpret the reported time points in a relative sense as early/intermediate/late post-shock time windows for comparing persistence across network configurations.

The plot reveals a general upward trend: as the number of feedback loops increases, the average aggregated symptom level tends to rise across all time points. However, this increasing trend begins to plateau when the number of loops exceeds 10 and reaches saturation beyond 17 loops, suggesting that additional feedback loops have minimal impact on further increasing symptom levels. Despite the overall upward trend, there is considerable variability in aggregated symptom levels within each network group with the same number of loops, as shown by the long and heavy tails of the boxplot. Although many networks with a high number of feedback loops tend to have elevated symptom levels, as indicated by the high median, some still exhibit very low levels, and vice versa (i.e., networks with fewer loops generally have lower symptom levels, although some of them show high levels). This broad variability is also evident in the far-right marginal distribution, which shows a relatively uniform spread with a slight peak at the lower end, resulting from the prevalence of networks with few or no loops.

The color-coded bars represent symptom levels at different time points, allowing us to track symptom progression over time. One thing that stands out is the presence of a hysteresis phenomenon, where the system does not readily return to a healthy state even after the stressor is removed [9]. This persistence can be attributed to the reinforcing nature of feedback loops, which sustain symptom activation. As the number of feedback loops increases, symptoms become more interconnected, leading to prolonged activation and slower recovery [14]. Symptom levels consistently peak at $t = 400$, shortly after the shock, and gradually decline thereafter. Figure 2 suggests that the primary difference is a systematic upward shift in post-shock symptom levels: networks with more feedback loops show higher aggregated symptom levels at each sampled post-shock time point. In other words, the distributions remain elevated both shortly after the shock and at later time points when compared at the same t , indicating more persistent symptom

FEEDBACK LOOPS IN SYMPTOM NETWORKS

activation. These findings suggest that networks with more feedback loops are more resistant to recovery, maintaining higher symptom levels over a prolonged period. This highlights the role of feedback structures in prolonging symptom activation and influencing recovery trajectories.

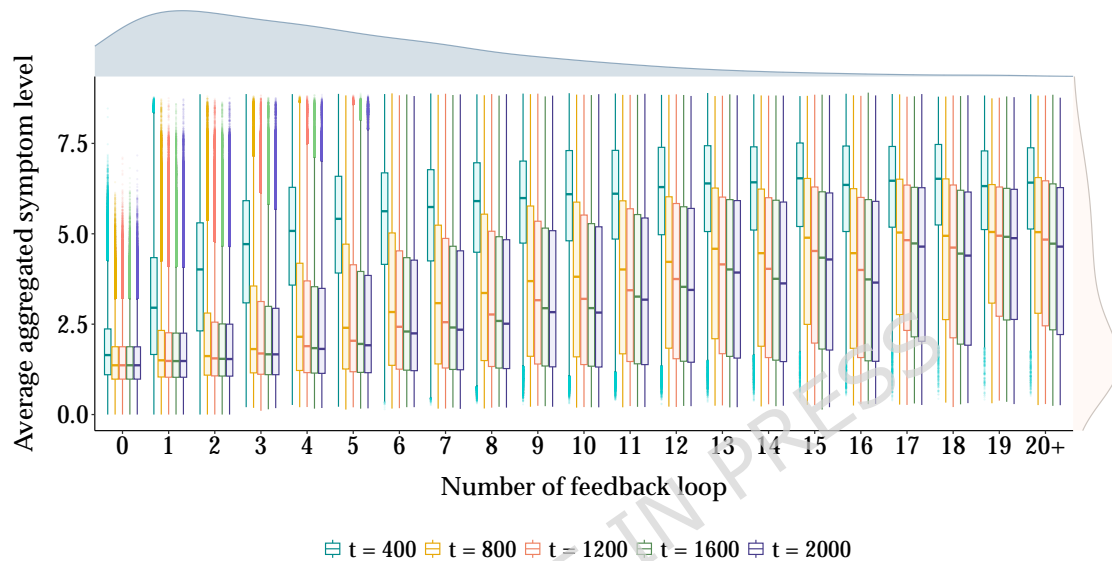


Figure 2

Distribution of average aggregated symptom levels throughout the simulations across different numbers of feedback loops within each unique network. A shock is introduced between $t = 50$ and $t = 350$. Symptom levels are recorded at five time points: $t = 400$ (teal), $t = 800$ (yellow), $t = 1200$ (red), $t = 1600$ (green), and $t = 2000$ (purple). The top panel illustrates the marginal distribution of the number of feedback loops, highlighting that networks with more than 10 loops are relatively rare. The right side of the plot shows the marginal distribution of the average aggregated symptom level, which ranges from approximately 0 (all symptoms deactivated) to 9 (all symptoms fully activated). The distribution peaks at low symptom levels because networks with few feedback loops are far more common. The average aggregated symptom level are calculated over 50 iterations.

Because networks with the same number of feedback loops can differ markedly in whether connectivity is broadly distributed or concentrated, we next examine weighted degree variability (σ_{tot}) as a complementary descriptor of network-wide connectivity balance. Figure 3 illustrates the relationship between average aggregated symptom levels and weighted degree variability (σ_{tot}) between networks at $t = 1200$, stratified by feedback-loop count; patterns were similar at

FEEDBACK LOOPS IN SYMPTOM NETWORKS

the other post-shock time points. The color gradient represents the level of overlap between feedback loops, with blue indicating low overlap and red indicating high overlap; overlap is low when loops are largely disjoint and increases as more loops share the same set of nodes. The lines in each subplot are fitted locally using the *loess* smoother to summarize the scatterplot patterns [27]. One key observation is the noticeable shift to the left in the distribution of σ_{tot} as the number of feedback loops increases from 1 to 20+. This suggests that networks with more feedback loops tend to have lower weighted degree variability. This pattern occurs because, in networks with many feedback loops, most nodes are involved in these loops, resulting in more evenly distributed connectivity. In contrast, networks with fewer feedback loops might have connections concentrated around a few nodes, leading to greater variability in connectivity.

In networks with fewer feedback loops (1 to 6 loops), symptom levels exhibit greater dispersion and variability, with no distinct pattern emerging. However, networks with 7 or more feedback loops reveal a distinct negative relationship between σ_{tot} and average aggregated symptom levels: As σ_{tot} increases, the average symptom level decreases. More evenly distributed connectivity allows activation to spread more easily throughout the network, maintaining higher aggregated symptom levels. In contrast, when connectivity is concentrated around a few nodes, activation spreads less effectively, resulting in lower symptom levels.

The color gradient further reveals that the feedback loop overlap level increases gradually as it radiates outward from the upper left corner of the plots towards the lower right. Networks with low overlap levels cluster in the upper left of most subplots, where higher symptom levels are observed. In contrast, networks with higher overlap levels dominate the lower right corner, generally showing lower symptom levels. This pattern suggests that extensive overlap among feedback loops tends to be associated with lower overall symptom levels. This finding is consistent with the saturation effect seen in Figure 2, where symptom levels plateau as the number of feedback loops increases. As the number of loops grows and they are more likely to overlap, they operate more cohesively as a single unit, contributing less to symptom levels compared to networks with distinct, non-overlapping feedback loops.

FEEDBACK LOOPS IN SYMPTOM NETWORKS

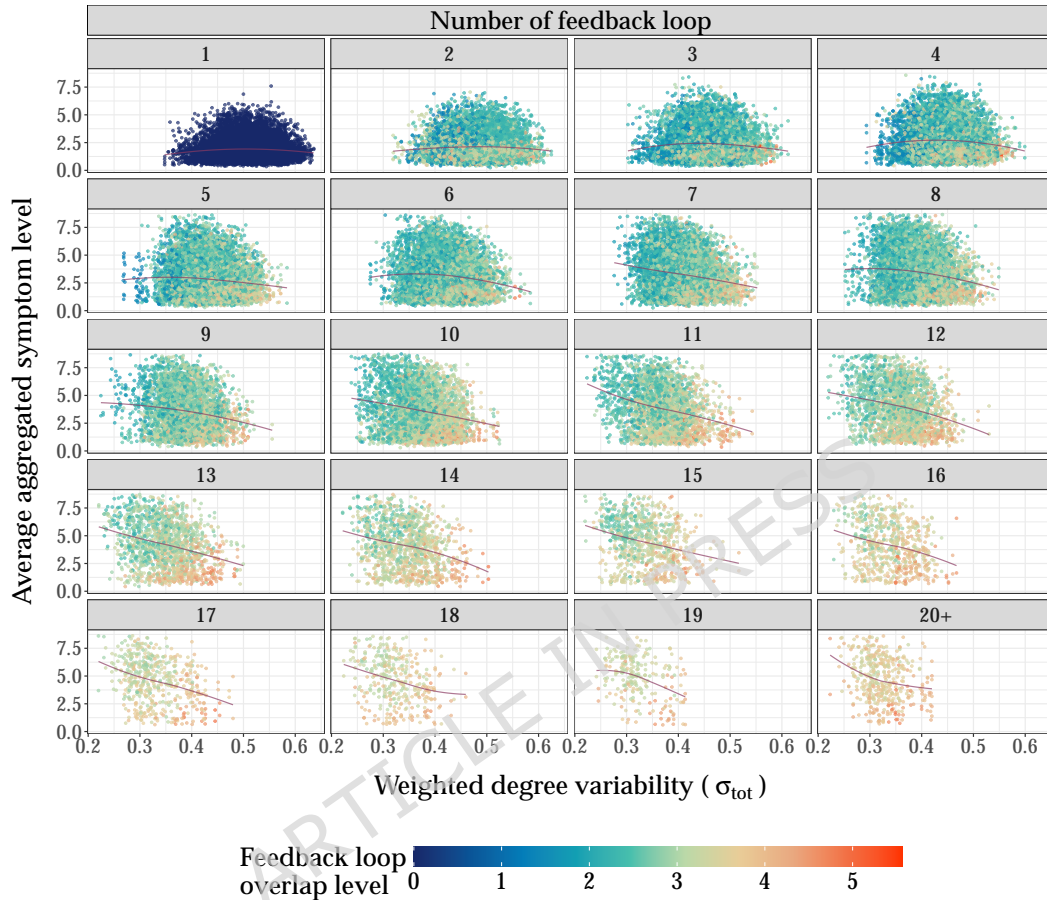


Figure 3

Average aggregated symptom levels across weighted degree variability (σ_{tot}) in networks, categorized by the number of feedback loops. The color represents the level of overlap between feedback loops, with blue indicating low overlap and red indicating high overlap. As the number of feedback loops increases, σ_{tot} generally decreases, shown by the data points shifting leftward as feedback loop counts increases. Networks with fewer feedback loops (e.g., 1 to 4 feedback loops) exhibit a more random spread with no distinct pattern. However, in networks with more than 5 loops, a clear trend emerges: higher σ_{tot} is associated with lower average aggregated symptom levels. Additionally, as the feedback loop overlap level increases, symptom levels tend to decrease. Low-overlap points are generally located in the upper left corner, with overlap levels increasing as they radiate outward.

FEEDBACK LOOPS IN SYMPTOM NETWORKS

Figure 4 summarizes the findings from Figures 2 and 3. A regression plane is fitted using the *loess* function with a neighborhood span of 0.75 [28]. To reduce visual clutter, only 5% of the data points (slightly more than 4,500 networks) are shown. In Figure 4 (a), we observe an upward trend in symptom levels as the number of feedback loops increases. The figure also shows that when the number of loops is low, the weighted degree variability (σ_{tot}) shows no distinct pattern. However, as the number of loops increases, a clear negative trend emerges: lower σ_{tot} is associated with higher average symptom levels. Figure 4 (b) emphasizes this negative interaction: the average level of symptoms increases with increasing number of feedback loops and decreasing σ_{tot} . In general, these results highlight that the interaction between the number of feedback loops and σ_{tot} significantly impacts symptom levels, providing a comprehensive view of how these topological features relate to symptom dynamics.

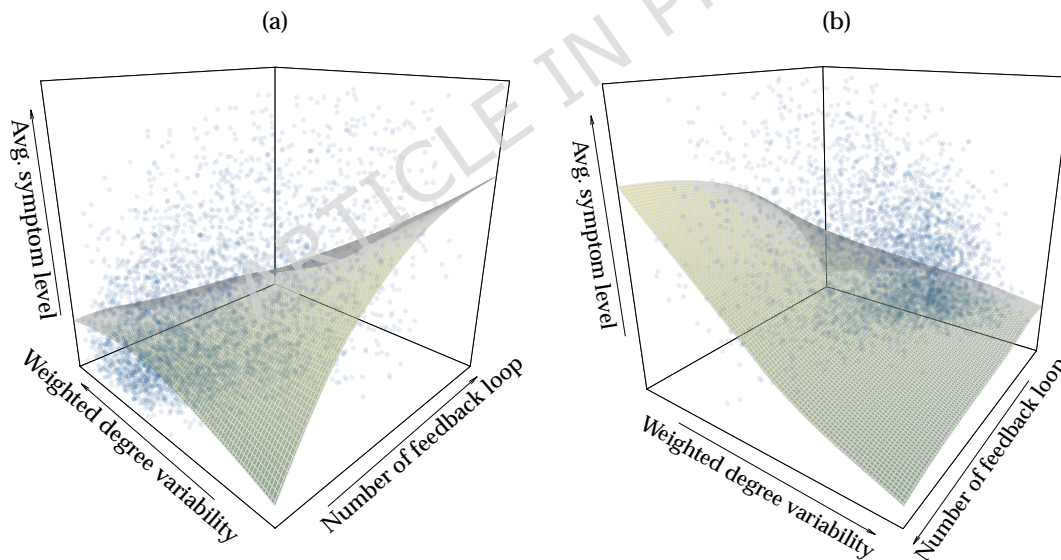


Figure 4

3D surface plots illustrating the interaction effects between the number of feedback loops and weighted degree variability (σ_{tot}) on the average aggregated symptom level. In view (a), we observe that when the number of feedback loops is high, a decrease in σ_{tot} leads to a higher average symptom level. However, as the number of feedback loops decreases, the effect of σ_{tot} becomes less significant. View (b) shows this relationship more clearly, where networks with a high number of feedback loops and low σ_{tot} correspond to higher average symptom levels. Furthermore, we observe a scarcity of networks with both a high σ_{tot} and a large number of feedback loops, resulting in a flat horizontal pattern on the right side of plot (b).

FEEDBACK LOOPS IN SYMPTOM NETWORKS

To verify that these patterns do not depend on a particular scaffold, we repeated the full pipeline on randomly generated skeletons matched on size and density but with different connectivity arrangements (Appendix D). The same qualitative results emerged—loop-driven increases with saturation under high overlap, and stronger persistence with more evenly distributed connectivity—indicating that the effects reflect general properties of cyclic organization rather than idiosyncrasies of a single network.

Feedback Loop Structure Analysis

We now take a closer look at the feedback loop structure at both the node and edge levels to identify patterns that strongly influence symptom dynamics. This analysis aims to pinpoint central nodes and edges that play a key role in feedback loop dynamics within the symptom network. To do this, we select 1,000 synthetic network configurations with the highest and lowest average aggregated symptom levels at various time points (we use four time points — $t = 800$, 1200, 1600, and 2000 — excluding $t = 400$ as it occurs too soon after the shock). We then examine the feedback loop structure in both network groups, focusing on the roles of individual nodes and edges.

Figure 5 shows the frequency of the nodes involved in the feedback loops for the two network groups, with red representing high symptom level networks and green representing low symptom level networks. The x-axis lists all nine nodes, while the y-axis shows their frequency. Since networks with high symptom levels generally have more feedback loops, we use the proportion of frequency to facilitate easier comparison with networks that have low symptom levels. The points represent the average frequency proportion across different time points, with error bars indicating one standard deviation. Interestingly, the figure reveals minimal differences between the high and low symptom level networks. In both groups, the symptoms *sad*, *ene*, and *glt* are the most frequently involved in feedback loops, with nodes *ene*, *glt*, and *con* slightly more frequently engaged in the low symptom level networks, while *slp* and *sui* are more involved in the high symptom level networks. This similarity suggests that identifying the central nodes involved

FEEDBACK LOOPS IN SYMPTOM NETWORKS

in feedback loops alone does not distinguish between high and low symptom level networks. Instead, other factors, such as the specific edges connecting the nodes and the directionality of those edges, may provide more meaningful insights.

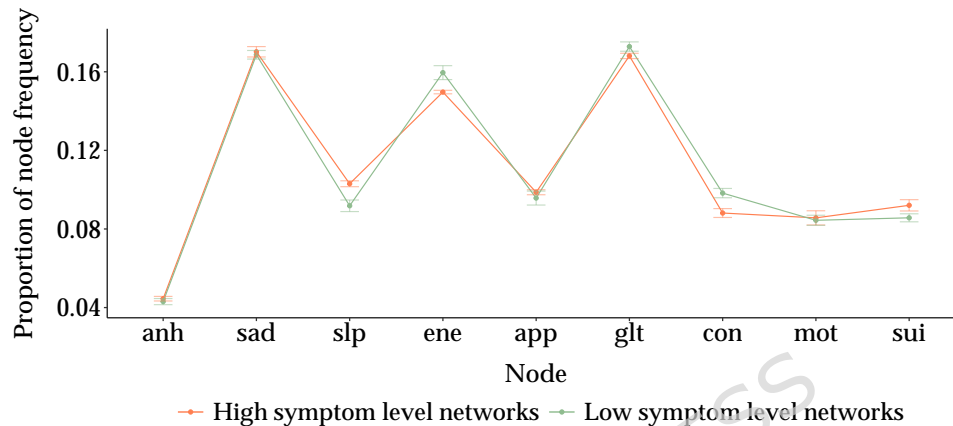


Figure 5

Frequency proportion of nodes involved in feedback loops in the top 1000 high symptom level networks (red) and bottom 1000 low symptom level networks (green). Points represent the average frequency proportion across different time points, with error bars showing one standard deviation. Overall, the patterns are similar, with the same nodes (e.g., sad, ene, glt) being most frequent in both groups.

Figure 6 shows the proportion of edge frequencies involved in feedback loops for the two network groups, with red representing high symptom level networks and green representing low symptom level networks. The x-axis lists the 32 distinct edges that are present across all network configurations, while the y-axis shows their frequency proportion. The points indicate the mean proportion for each edge across different time points, while the error bars depict one standard deviation. Edges are ordered according to their frequency in the high symptom level networks. The top 13 edges in terms of frequency in this network are highlighted with larger, solid points. For comparison, the top 13 most frequent edges in the low symptom level networks are also marked with larger solid points. The choice of the top 13 edges is informed by the distribution of edge frequencies, which display an inflection point resembling the elbow method heuristic commonly used to identify significant thresholds [29].

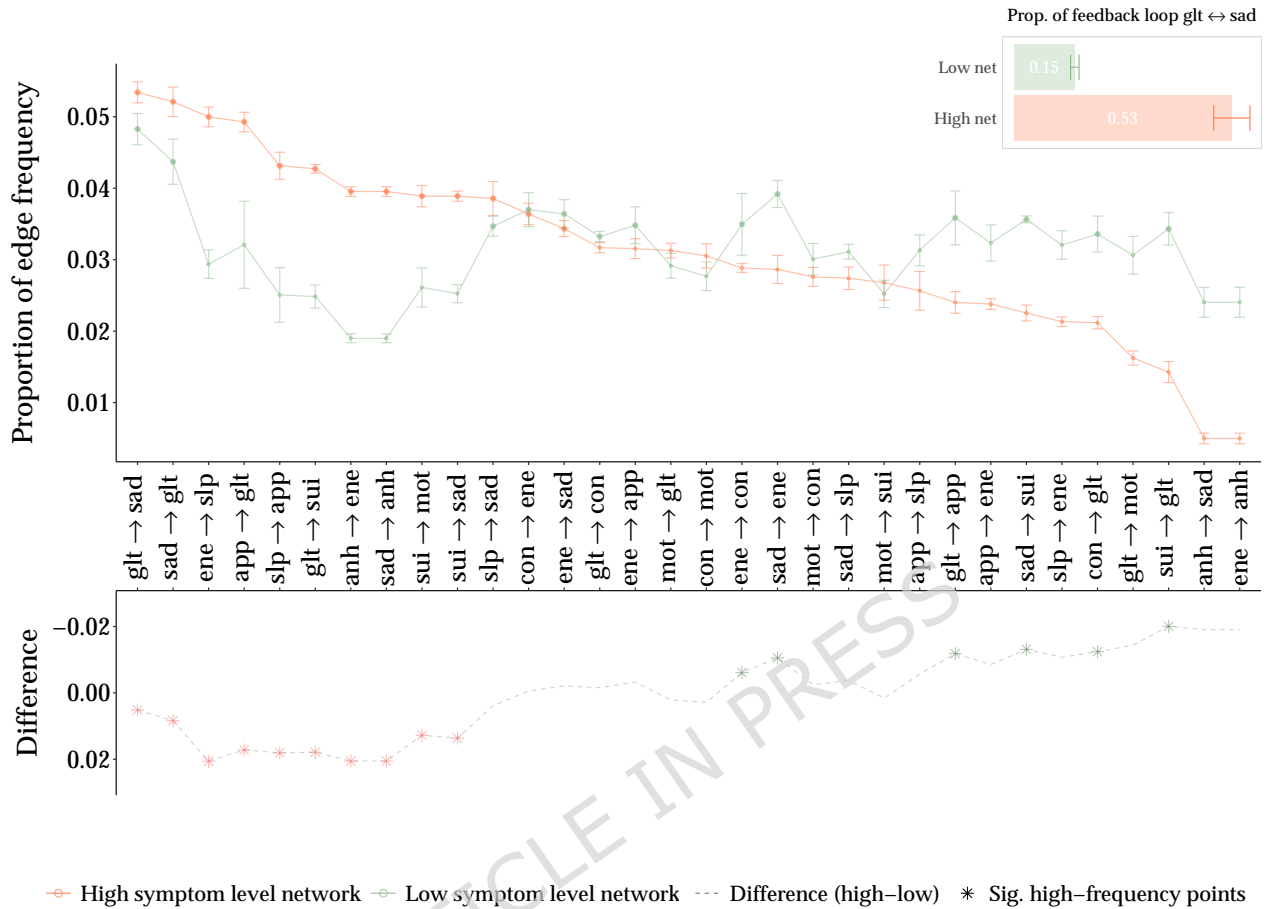
FEEDBACK LOOPS IN SYMPTOM NETWORKS

One key observation is that the variability (standard deviation) in edge frequencies is broader in low symptom level networks compared to high symptom level networks, indicating more diverse edge involvement in feedback loops within the low symptom group. Conversely, in high symptom level networks, edge frequencies are more consistent across different time points, resulting in smaller standard deviations. This suggests that specific edges consistently play a prominent role in the high symptom group. Certain edges, such as $glt \rightarrow sad$, $sad \rightarrow glt$, $slp \rightarrow sad$, $con \rightarrow ene$, and $ene \rightarrow sad$, are frequently involved in loops in both network groups. However, other highly frequent edges (represented by solid points), are unique to each group, highlighting distinct interaction patterns between the high and low symptom level networks.

The lower line plot highlights the differences in edge frequency proportions between the high and low symptom level networks. The values represent the proportion in high symptom level networks minus the proportion in low symptom level networks; thus, positive values indicate edges more common in high symptom networks, while negative values indicate higher frequencies in low symptom networks. Note that the y-axis is inverted. Edges with descriptively greater frequency in one group — where the standard deviations do not overlap — are marked with asterisks (*). In total, 10 edges are more frequent in high symptom level networks, while 6 are more frequent in low symptom level networks. These contrasts are descriptive summaries rather than results of formal statistical testing. This finding suggests that certain feedback loops and connections are associated with sustained symptom levels, potentially highlighting the structural requirements for severe symptoms to manifest. The bar plot in the top right corner shows the average proportion of the $sad \rightleftharpoons glt$ feedback loop in each network group, which we will explore further in the next section with network visualizations of these frequent edges.

Figure 7 provides a visual representation of the 13 edges most frequently involved in feedback loops for both the high and low symptom level networks. Panels (a) and (b) display these frequent edges for each network group, respectively. Solid lines indicate the most commonly observed edges within each group, while dashed lines highlight edges with descriptively higher frequency in one group compared to the other—corresponding to those

FEEDBACK LOOPS IN SYMPTOM NETWORKS

**Figure 6**

Proportion of edge frequency involved in feedback loops in the top 1000 high-symptom-level networks (red) and bottom 1000 low-symptom-level networks (green). Each point represents the average proportion of occurrences for a specific edge across all time points, with error bars indicating one standard deviation. Edges are ordered by their frequency in high-symptom-level networks. Larger solid dots highlight the 13 most frequently observed edges in each group. The differences between the two groups (high – low symptom networks) are visualized in the bottom plot with a gray dashed line. Positive values indicate edges more frequently observed in high-symptom networks, while negative values reflect edges more commonly present in low-symptom networks. Note that the y-axis is inverted. Asterisks indicate edges with descriptively higher frequency in one group, based on non-overlapping standard deviations. The bar plot in the top right corner displays the average proportion of the sad \leftrightarrow glt feedback loop in each network group across all time points, with error bars representing one standard deviation. This loop appears more frequently in the high-symptom networks (mean = 0.53, SD = 0.04) than in the low-symptom networks (mean = 0.15, SD = 0.01).

FEEDBACK LOOPS IN SYMPTOM NETWORKS

marked with asterisks in Figure 6, based on non-overlapping standard deviations. In the high symptom level network (Panel a), frequent edges are dispersed throughout the network. The network reveals several prominent feedback loops, including a large loop that encompasses nearly all nodes, $sad \rightarrow anh \rightarrow ene \rightarrow slp \rightarrow app \rightarrow glt \rightarrow sui \rightarrow sad$, as well as smaller loops such as $sad \rightarrow glt \rightarrow sui \rightarrow sad$ and $sad \rightarrow anh \rightarrow ene \rightarrow sad$. In contrast, the low symptom level network (Panel b) shows more localized structure, with frequent edges mainly concentrated around four central nodes: sad , ene , glt , and con . Peripheral nodes such as slp , anh , and mot are less involved in feedback loops, indicating more constrained cyclic dynamics. The largest feedback loop in this network involves five nodes: $sad \rightarrow sui \rightarrow glt \rightarrow con \rightarrow ene \rightarrow sad$, with other loops being smaller and more centered around these core nodes. This aligns with the observations from Figure 5, where these nodes are more frequently involved in feedback loops in the low symptom level networks. When examining the edges that appear with notably higher frequency (indicated by dashed lines), it becomes clear that these edges are more prevalent in high symptom level networks and tend to span a broader range of nodes. In contrast, fewer such edges are observed in low symptom level networks, suggesting less structural regularity in the feedback loops associated with lower symptom dynamics.

Note that the bidirectional edges observed in Panel (b) do not necessarily represent true feedback loops. Instead, these edges in the low symptom level network indicate that both directions of the connection are often involved in feedback loops, but not as part of a direct loop structure. For instance, the edges between sad and glt in the low symptom level network suggest that each direction ($sad \rightarrow glt$ and $glt \rightarrow sad$) frequently participates in cycles, though not necessarily together as a distinct dyadic loop ($sad \rightleftharpoons glt$). To clarify this, we analyzed the presence of the actual $sad \rightleftharpoons glt$ feedback loop in both network groups. As shown in the top right corner of Figure 6, this specific loop appears in over 50% of cases in the high symptom level networks, but only about 15% in the low symptom level networks; error bars denote one standard deviation. Although both edges— $sad \rightarrow glt$ and $glt \rightarrow sad$ —are commonly involved in feedback loops across network types, the full bidirectional loop is markedly more prevalent in high

FEEDBACK LOOPS IN SYMPTOM NETWORKS

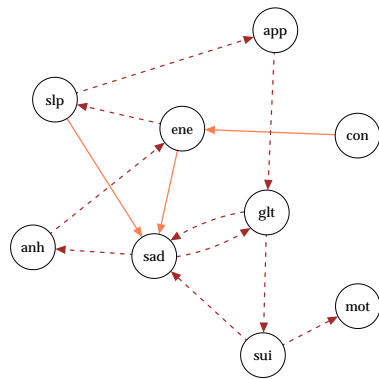
symptom networks. This pattern suggests that the *sad* \rightleftharpoons *glt* dyad may play a particularly prominent role in sustaining elevated symptom levels, potentially functioning as a core regulatory mechanism in depressive dynamics.

A potential concern is that these differences are merely due to variations in the number of feedback loops, with high symptom level networks having more diverse loops, and thus more varied structures, than low symptom level networks. Although this is generally true, as Figure 2 shows, symptom levels can vary widely even within networks that have the same number of feedback loops. For example, Panels (c) and (d) each depict example networks with 15 feedback loops but differing symptom levels. In the high symptom level network, shown in Panel (c), the feedback loop structure closely mirrors that of the frequent edges in Panel (a), featuring a large, prominent loop along with several smaller ones. Conversely, the low symptom level network, shown in Panel (d), presents multiple smaller, less interconnected loops, reinforcing the idea that certain network structures, beyond just the quantity of feedback loops, could play a critical role in determining symptom severity. While Panels (c) and (d) serve as illustrative examples, they represent a broader pattern observed across the 1,000 networks analyzed, ensuring the findings are not an artifact of selective sampling.

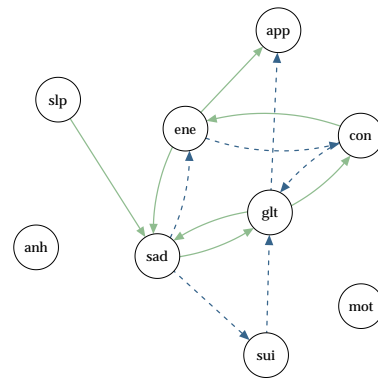
Lastly, we analyzed the frequency of each unique feedback loop in both network groups, treating loops as equivalent if they involved the same set of nodes, regardless of traversal order. The results, detailed in Appendix B, showed that the most frequently occurring loops largely overlap with the edges identified in Figure 7, reinforcing the consistency of these structural patterns. Broadly, this comparison suggests a structural distinction between the two network groups: high symptom level networks tend to exhibit more extensive and distributed feedback structures, while low symptom level networks are characterized by more localized and narrowly concentrated loops. This pattern may indicate that larger-scale, overlapping feedback configurations are more closely associated with elevated symptom levels, in contrast to the more limited feedback dynamics observed in networks with lower symptom severity.

To evaluate whether our findings depend on the specific empirical adjacency matrix, we

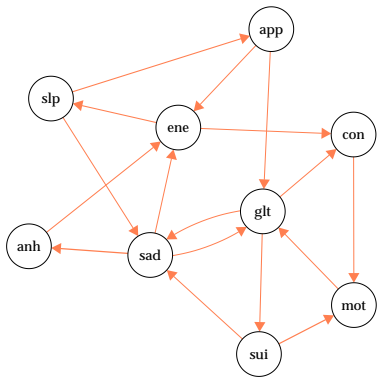
FEEDBACK LOOPS IN SYMPTOM NETWORKS



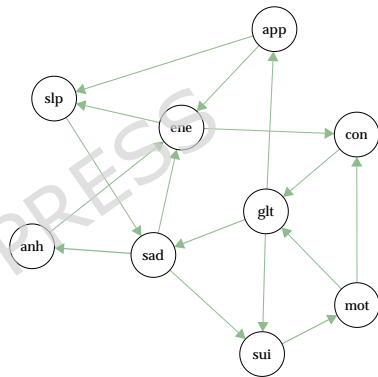
(a) Frequent edges in high symptom level networks



(b) Frequent edges in low symptom level networks



(c) An example network with 15 feedback loops resulting in high symptom level



(d) An example network with 15 feedback loops resulting in low symptom level

Figure 7

Visualization of the most frequent edges involved in feedback loops and example networks illustrating differences in loop structure between high and low symptom level networks. **(a)** High symptom level networks: Solid lines indicate the 13 edges most frequently involved in feedback loops, while dashed lines mark edges that appear more frequently in high symptom networks relative to low symptom networks. These networks feature dispersed edges forming both large interconnected loops and smaller localized loops. **(b)** Low symptom level networks: Solid lines represent the 13 most frequent edges. Here, dashed lines highlight edges more common in low than in high networks. These networks feature edges that are more localized, concentrated around core nodes (*sad*, *ene*, *gt*, *con*), with peripheral nodes (*anh*, *mot*) less involved. **(c)** Example network (15 loops, high symptom level): This network features a large interconnected feedback loop involving nearly all nodes, alongside multiple smaller loops, consistent with the patterns observed in high symptom level networks. **(d)** Example network (15 loops, low symptom level): Despite having the same number of loops, this network displays less interconnectivity, with feedback loops concentrated among fewer nodes—illustrating a structural profile associated with lower symptom levels.

FEEDBACK LOOPS IN SYMPTOM NETWORKS

conducted a complementary set of simulations on randomly generated network skeletons with the same size and density but different edge arrangements and weights (Appendix D). These replications reproduced the key patterns observed in the main analysis: symptom levels increased with the number of feedback loops but plateaued as overlap grew, and networks with more evenly distributed connectivity sustained higher symptom persistence. This demonstrates that the effects of cyclic structure and connectivity balance are not artifacts of a single reference network, but generalize across diverse global connectivity patterns.

Empirical Result

To assess external consistency, we estimated patient-specific directed symptom networks from an independent clinical time series using PCMCI+ and compared their edge motifs with those from the simulations (see Methods for data and analysis details). For each patient, we obtained a directed graph; collapsing lag order, we computed cross-patient frequencies for each directed edge and contrasted the most recurrent motifs with simulation-derived patterns.

Figure 8 presents the 10 most frequent edges across all patients, visualized as a network, considering only directed edges in the analysis. Time lags are not differentiated, meaning edges such as $A_{t-1} \rightarrow B_t$ and $A_{t-2} \rightarrow B_t$ are treated as equivalent. Interestingly, these edges largely align with those observed in the high symptom level network from our simulation, as illustrated in Figure 7. Five of the top 10 edges align with those identified in the high symptom level networks from the simulations. However, two edges ($con \rightarrow slp$ and $app \rightarrow con$) are absent from both high and low symptom level networks, as they are not part of the original reference network structure used in the simulations. Additionally, two edges ($anh \rightarrow sad$ and $con \rightarrow mot$) are uncommon in either simulated network type, while one edge ($ene \rightarrow app$) is characteristic of low symptom level networks.

Despite these differences, the frequent edges in the empirically derived network show considerable alignment with the patterns observed in high symptom level networks from the simulations. Particularly, the dyadic loop between $sad \rightleftharpoons glt$, a defining feature of high symptom

FEEDBACK LOOPS IN SYMPTOM NETWORKS

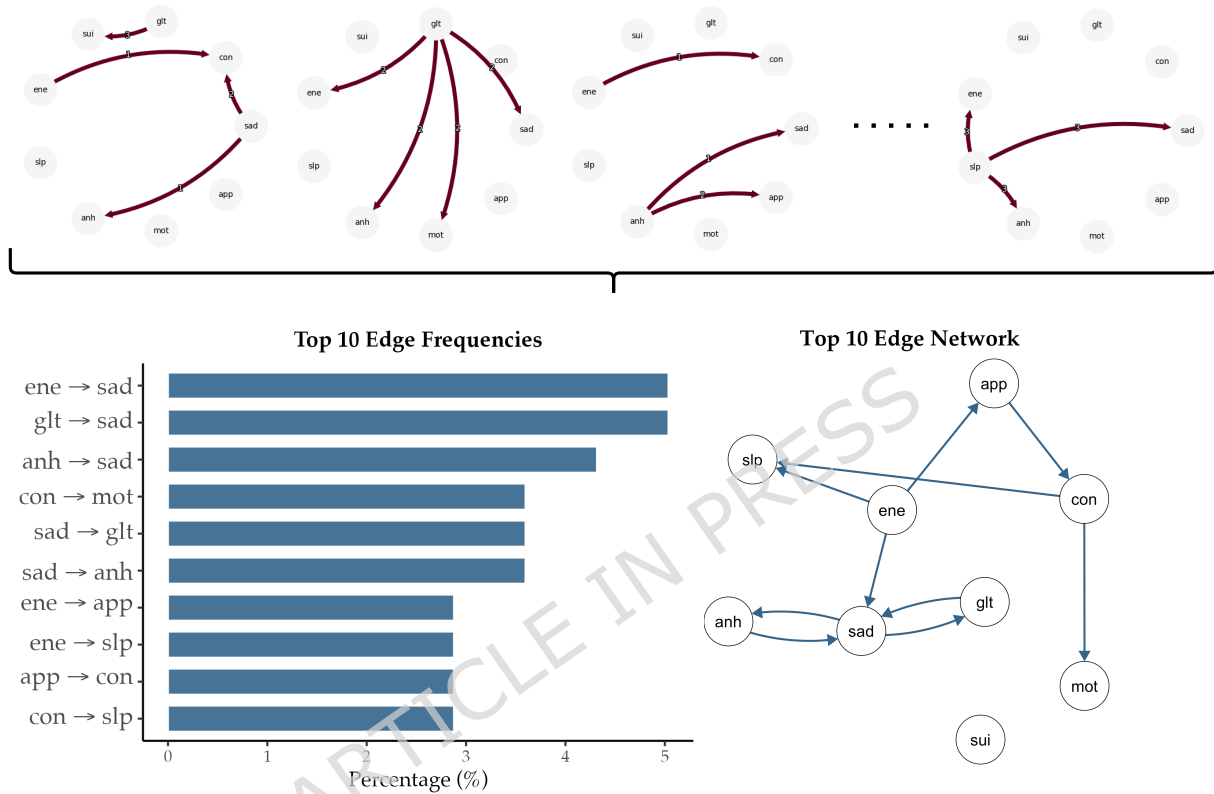
level networks, also appears prominently in the empirical networks. While the proportion of frequent edges remains low (around 5%), this is consistent with the simulated networks, where edge frequency is similarly around 5%. For more discussion on why this proportion is low yet meaningful, see Appendix C. Overall, these findings indicate external consistency between the simulation-derived patterns and the network features estimated from individual patient time series. This empirical alignment suggests that the simulation results capture structural properties that also arise in real-world symptom dynamics, supporting the use of simulation-derived ensembles as a tool for generating and prioritizing hypotheses about symptom-network behavior.

Discussion

In this paper, we explored the role of feedback loops in the dynamics of symptoms within mental disorder networks, focusing on how the number and structure of these loops impact the severity and persistence of symptoms. By examining the topological features of symptom networks, our study offers critical insights into how the structure of the network influences overall symptom levels and helps explain sustained high depression states.

Our findings revealed a clear relationship between the number of feedback loops in a network and the aggregated level of symptoms. Consistent with previous studies [9, 14], networks with a greater number of feedback loops exhibited and maintained higher symptom levels over time. This suggests that feedback loops act as reinforcing mechanisms, amplifying symptom activation. However, this relationship plateaued as the number of loops exceeded approximately ten, indicating a saturation effect. This effect may result from increased overlap among loops, which reduces the distinct contribution of each additional loop to the network's overall reinforcement capacity. As shown in Figure 3, highly overlapping loops become increasingly interdependent, weakening the influence of any individual loop. Clinically, this may explain why mental disorders often persist despite attempts to reduce symptom intensity. A few loop disruptions may not suffice; rather, interventions must break enough key cycles to prevent symptom reactivation. This perspective aligns with clinical observations of depression's chronic

FEEDBACK LOOPS IN SYMPTOM NETWORKS

**Figure 8**

Using the PCMCI+ algorithm, we estimate a causal graph for each of the 254 patients. The top panel displays example network graphs for individual patients. From these graphs, we identify all unique edges and calculate their frequencies. In computing edge frequencies, we do not differentiate between time lags, meaning edges such as $A_{t-1} \rightarrow B_t$ and $A_{t-2} \rightarrow B_t$ are treated as equivalent. The bar plot on the left illustrates the top 10 most frequent edges across all patient graphs, while the network visualization on the right represents these edges. Interestingly, 5 of these top 10 edges (i.e., $ene \rightarrow sad$, $glt \rightarrow sad$, $sad \rightarrow anh$, $sad \rightarrow glt$, $ene \rightarrow slp$) align with the frequent edges observed in high symptom level networks, as shown in Figure 7. Especially, the dyadic loop between $sad \rightleftarrows glt$ stands out, which is a key feature of high symptom level networks.

FEEDBACK LOOPS IN SYMPTOM NETWORKS

nature and its frequent relapse, especially among individuals with more severe or treatment-resistant forms [30–32].

Further insights were obtained by analyzing the weighted degree variability (σ_{tot}) within these networks. Networks with lower σ_{tot} , indicating more evenly distributed connectivity, tend to enable more uniform symptom activation across the network, sustaining higher overall symptom levels. In contrast, networks with higher σ_{tot} exhibit more uneven connectivity, where certain nodes may dominate network dynamics. Among networks with the same number of feedback loops, the observed negative relationship between σ_{tot} and symptom levels suggests that a more evenly distributed connectivity makes the network more robust in maintaining high symptom levels. Conversely, networks with greater variability in connectivity are more vulnerable to disruptions at specific nodes, indicating that targeted interventions at these key nodes could significantly reduce symptom levels. While, in this paper, we worked under a philosophy of shared causal pathways across individuals, these may, in fact, differ. In such a case, our finding underscores the importance of comprehensive interventions in networks with evenly distributed connectivity. In such systems, it may be necessary to target multiple feedback loops and nodes simultaneously to disrupt the network's cohesive structure and reduce high symptom levels. Effective strategies could involve disrupting network cohesion or altering the balance of connectivity to destabilize the network and reduce the persistence of symptoms.

Delving deeper, our local analysis revealed that it is not merely the presence of feedback loops that matters, but their specific structure. Interestingly, the participation of individual nodes in feedback loops did not differ substantially between high- and low-symptom-level networks. Rather, differences in symptom severity appeared to stem from the specific edges involved and how they were arranged within loop structures. High-symptom-level networks were characterized by more widespread and extended feedback configurations, forming larger and more interconnected sets of loops. In contrast, low-symptom-level networks displayed more localized feedback, often concentrated around a few central nodes with limited reach. These findings highlight a broader conceptual point. While much prior network research has emphasized

FEEDBACK LOOPS IN SYMPTOM NETWORKS

identifying "central" nodes as intervention targets, recent critiques have raised serious concerns about the stability and interpretability of centrality measures in psychometric networks [33–35]. Our results align with these critiques: node involvement alone did not meaningfully distinguish network behavior across symptom levels. Instead, the dynamics were shaped by how edges formed and interacted within feedback loops. This suggests that effective interventions may be better guided by targeting key structural configurations—particularly those involving critical loops—rather than relying on centrality metrics.

The implications of these results are necessarily indirect, but they can still inform clinical mechanistic reasoning about symptom persistence. In particular, our loop-architecture perspective clarifies three conceptually distinct levels at which change might be pursued: (i) individual symptoms (node-level targets), (ii) specific symptom-to-symptom relations (edge-level targets), and (iii) broader reinforcing configurations in which multiple relations jointly sustain one another (feedback-structure targets). Even when these levels are not directly translatable into concrete intervention protocols, it helps clarify why reducing a single symptom may not shift the system if the underlying reinforcing structure remains intact, and why two patients with similar symptom severity could differ in persistence depending on whether reinforcement is localized to a small motif versus distributed across overlapping loops.

One particularly illustrative case is the dyadic *sad* \rightleftharpoons *glt* loop, which consistently emerged as a central feature of high-symptom-level networks. This loop reflects a clinically plausible dynamic: sadness often heightens vulnerability to guilt, particularly through self-blame and rumination [36], while guilt, in turn, can intensify sadness—creating a mutually reinforcing emotional cycle [37, 38]. Although this specific loop has not been extensively modeled in empirical network studies, a growing body of evidence supports its psychological and neural relevance. For instance, Zahn et al. [39] found that self-blaming emotions like guilt are strongly associated with depression and frequently persist even after other symptoms subside. Neuroimaging studies further show that individuals with current or remitted depression exhibit sustained activation in brain regions implicated in both guilt and sadness during guilt-related

FEEDBACK LOOPS IN SYMPTOM NETWORKS

processing [40, 41]. These findings suggest that guilt and sadness share overlapping cognitive-affective pathways and may co-activate persistently in depressive states. While not always framed explicitly as feedback loops, such dyadic symptom pairings likely function as tightly coupled mechanisms that reinforce one another over time. The prominence of the sad–guilt loop in our simulation results is therefore consistent with both theoretical models and empirical patterns, pointing to its potential role as a core driver of symptom persistence in severe depression.

Our empirical analysis supports these findings. Directed networks derived from patient data closely resembled the high-symptom-level networks observed in simulations. Among the 10 most frequently occurring edges in the empirical networks, half corresponded to those observed in high-symptom-level networks. Additionally, dyadic loops such as $sad \rightleftharpoons glt$ again appear prominently in the empirical data. This correspondence is particularly striking given the independent sources of the empirical and simulated data. These results suggest that specific structural patterns underpin symptom dynamics, with severe symptoms in real-world contexts likely driven by dyadic loops and wide-spreading, interconnected feedback structures. Together, our findings suggest that effective interventions should not merely aim to reduce overall connectivity, but should prioritize disrupting key feedback loops and high-impact connections. Targeting these structural features could destabilize the network and reduce the persistence of symptoms. Although our primary simulations held the empirical adjacency matrix constant to isolate the role of directional structure, Appendix D demonstrates that the same phenomena emerge in randomly generated networks with varied global connectivity patterns. This robustness analysis indicates that feedback-loop architecture and connectivity balance exert systematic effects on symptom persistence, above and beyond global connectivity strength.

While our study provides valuable insights into how feedback loop structures shape symptom dynamics, several limitations warrant discussion. First, the reference network used in our simulations, although grounded in empirical data [16], remains a stylized abstraction. It does not fully capture the complexity and heterogeneity of real-world symptom interactions in mental

FEEDBACK LOOPS IN SYMPTOM NETWORKS

disorders. In addition, because the reference matrix contains only positive weights, the present simulations focus on reinforcing interactions; extending the framework to signed (mixed positive/negative) edges that incorporate inhibitory interactions is an important direction for future work. A particularly important limitation is the underrepresentation of multiple dyadic feedback loops, which emerged as critical structures in both our simulations and empirical analysis. Given their apparent role in sustaining symptom severity, future work should investigate their prevalence and functional impact across more diverse and complex network configurations.

Another key limitation lies in the empirical dataset. Due to administrative and data-sharing restrictions, we were unable to access the original continuous or ordinal symptom ratings and were limited to using dichotomized symptom data. This reduction in measurement granularity inherently limits analytical sensitivity, as binary encoding discards meaningful gradations in symptom severity. As a result, subtle but clinically relevant dynamics in symptom progression may have been obscured. The temporal structure of the dataset also posed constraints. Each patient's time series included, on average, only 26 observations, with relatively long intervals between measurement points [42]. This limited temporal resolution likely hindered the detection of short-term symptom transitions and contributed to the sparsity and instability of the estimated networks. Furthermore, the data were drawn from a structured psychotherapy trial, which may not reflect the symptom dynamics of broader, untreated, or community-based populations—thus limiting the generalizability of our findings.

Beyond data constraints, the causal discovery method employed—PCMCI+—relies on strong assumptions, including causal sufficiency and faithfulness. These assumptions are often difficult to meet in psychological data, where latent confounders, measurement error, and complex feedback dynamics are common. As a result, we interpret the estimated empirical networks as exploratory and hypothesis-generating, serving as a complement to our simulation findings rather than as definitive or confirmatory evidence.

Finally, we clarify that our simulations are not based on a single assumed causal network. Rather, we used a correlation-based network—drawn from empirical data—as a scaffold for

FEEDBACK LOOPS IN SYMPTOM NETWORKS

generating a family of directed networks. While correlation does not imply causation, prior work suggests that empirical symptom correlations often reflect latent or underlying causal processes [20, 21]. Accordingly, we varied edge directions across all feasible configurations consistent with this skeleton to systematically explore how feedback loop structure relates to symptom dynamics. Our findings were robust across this entire ensemble of networks, underscoring that the observed effects are not an artifact of any specific causal assumption.

Looking ahead, several methodological improvements could substantially strengthen future research. One important direction involves refining the reference network structure to better capture a broader and more realistic range of symptom interaction patterns—particularly the role of dyadic feedback loops, which were underrepresented in our current model. Enhancing structural realism in the network would improve both the interpretability and the clinical relevance of simulated dynamics. Improving the quality of empirical data is also critical. Incorporating richer, high-frequency temporal data would allow for more precise estimation of edge directionality by revealing fine-grained sequences of symptom activation. In the present study, our time-series data were limited to an average of only 26 observations per patient, with relatively long intervals between measurements [42]. This limited temporal resolution likely obscured fast-evolving dynamics. More granular data would support the application of temporal modeling frameworks—such as (multilevel) vector autoregressive (VAR) models—enabling more accurate detection of symptom transitions and providing a stronger empirical foundation for network-based inferences [20]. In parallel, advances in causal discovery methods offer additional opportunities. Traditional statistical network approaches often fall short in establishing causal directionality [43], and many existing methods are limited to acyclic structures [44]. Applying algorithms like PCMCI [22] to higher-resolution time-series data may yield more reliable estimates of both lagged and contemporaneous feedback mechanisms. Furthermore, recent techniques capable of inferring causal directions from cross-sectional data—such as cyclic causal discovery (CCD), fast causal inference (FCI), and cyclic causal inference (CCI)—present promising alternatives in settings where longitudinal data are unavailable or difficult to collect

FEEDBACK LOOPS IN SYMPTOM NETWORKS

[45–48]. Incorporating these data and methodological advances could substantially improve the realism and robustness of both reference networks and simulation models. Ultimately, this would deepen our understanding of the dynamic architecture of mental disorders and support the development of more targeted and effective intervention strategies.

Feedback loops have long been recognized as an important aspect in the study of mental health, but their specific roles and impacts, particularly in relation to structural differences, have remained somewhat unclear. This study underscores the importance of feedback loop architecture in sustaining and intensifying symptom levels within mental disorder networks. By identifying particular configurations—especially those involving dyadic and highly interconnected loops—that are associated with persistent symptoms, we provide a foundation for designing more targeted and structurally informed interventions. Disrupting a single feedback loop may already be challenging; addressing systems characterized by multiple, overlapping loops requires a broader and more strategic approach. We hope this work encourages further research into pinpointing the most influential feedback structures, with the goal of informing clinical strategies that disrupt maladaptive symptom dynamics. Such efforts could pave the way for more effective and enduring interventions in the treatment of mental health conditions.

Methods

To explore the impact of feedback loops on symptom persistence, we selected a realistic network structure derived from empirical data [16]. Constructed by aggregating sub-population partial correlation networks, this symptom network skeleton captures core interdependencies between symptoms, providing a concrete foundation for our analysis. While the overall structure of depressive symptom networks is robust—consistently observed across empirical studies—the causal direction of symptom interactions remains largely unknown [49–51]. In Park, Waldorp, and Vasconcelos [16], directionality was inferred based on literature and theoretical assumptions. To systematically address this uncertainty, we generate all possible directed configurations—referred to as *synthetic networks*—by flipping the direction of every edge. This

FEEDBACK LOOPS IN SYMPTOM NETWORKS

approach allows us to examine how different feedback loop structures shape symptom dynamics while accounting for all potential directional arrangements.

We then examined the topological features of these synthetic networks to understand how feedback dynamics evolve across various network configurations. We hypothesize that the structure and number of feedback loops — whether it involves a single cycle, multiple loops, or how much overlap exists between them — casually influence symptom progression. A core concept in cyclic structure is that of a "*cyclegroup*" [52], a minimal set of cycles that captures all possible transitive closures of intersecting cycles. This means that cycles in a directed cyclic graph can overlap or interconnect in complex ways, which ultimately influences the system's overall dynamics. Spirtes [52] emphasizes that understanding these cycles and their interactions is crucial for analyzing feedback systems. Different cycle configurations, including their overlaps, may substantially affect how the system behaves.

When applying these insights to mental health networks, feedback loops — such as those between symptoms like sadness and sleep disturbances in depression — give rise to different cycle structures, some of which overlap. Understanding whether a network contains isolated cycles or overlapping ones, as well as the nature of these cycles — whether they involve many or few nodes, or are larger or smaller in scope — is crucial. Overlapping cycles, in particular, may result in more persistent symptoms, and the structure of these loops could significantly influence the course of recovery or the persistence of the disorder. By examining all possible network configurations within a robust network skeleton, we aim to investigate how feedback loops' impact varies depending on their structural characteristics — including the number of loops, the extent of overlap, and the balance of connectivity across nodes. This approach emphasizes the complexity of cycle structures within feedback loops, offering a more nuanced understanding of how symptom networks evolve and persist over time. This section (i) introduces the SDE-based symptom-dynamics model, (ii) describes how we generate an ensemble of directed network configurations from the empirical skeleton, and (iii) details our procedures for detecting feedback loops and computing topological metrics (loop count, overlap, connectivity balance, and

FEEDBACK LOOPS IN SYMPTOM NETWORKS

node/edge participation). We then provide the empirical dataset specifications and the PCMCI+ causal discovery protocol used to estimate patient-specific directed networks for assessing external consistency with the simulation results.

Reference Network and Symptom Dynamics Model

Figure 1 illustrates the reference network structure used in this study. Originally developed from empirical evidence presented in Park, Waldorp, and Vasconcelos [16]. It consists of nine symptom nodes, aligned with the PHQ-9 questionnaire convention [53], and includes 17 edges. A dyadic feedback loop between two nodes (*sad* \rightleftharpoons *guilt*), highlighted in orange, is retained from the original network. While we use its skeleton (undirected version), this bi-directional connection — linking the two most central, high-degree nodes — is preserved to explore the impact of feedback involving only two symptoms. In the figure, the color saturation and edge width represent the relative weights of the connections, as detailed in the weighted adjacency matrix A .

This study builds on the symptom dynamics model for depressive symptoms introduced in Park, Waldorp, and Vasconcelos [16]. The model employs stochastic differential equations (SDEs) to formalize interactions between symptoms within a continuous-time dynamical framework. It can reproduce key phenomena such as bistability and hysteresis [9, 14, 25, 54, 55], making it a useful platform for investigating how feedback structures influence symptom progression and persistence.

This study builds on the symptom dynamics model for depressive symptoms introduced in Park, Waldorp, and Vasconcelos [16]. The model employs stochastic differential equations (SDEs) to formalize the interactions between symptoms, making it one of the few computational models that can effectively model the complex dynamics of mental disorders within a continuous framework. It incorporates key phenomena such as bistability and hysteresis [9, 14, 25, 54, 55], providing a robust platform for investigating how feedback loops influence symptom progression and persistence over time. The system of SDEs governing symptom interactions is shown in

FEEDBACK LOOPS IN SYMPTOM NETWORKS

Equation 1:

$$dS_i = S_i(1 - S_i) \left(\beta_i + \alpha_{ii}S_i + \sum_{\substack{j=1 \\ j \neq i}}^9 \alpha_{ji}S_j(1 + \delta_i S_i^2) \right) dt + \sigma_i dW_i, i = 1, 2, \dots, 9. \quad (1)$$

Equation 1 models the rate of change of each symptom, S_i ($i = 1, \dots, 9$), as dS_i/dt . This change is driven by two components: the symptom's intrinsic dynamics, represented by $S_i(1 - S_i)$, and interactions with connected symptoms, captured within the equation's large brackets. The term $S_i(1 - S_i)$ also constrains symptom levels to a range between 0 (inactive) and 1 (active), consistent with bounded scales used in empirical symptom measurement [56, 57]. The interactions with connected symptoms are influenced by three key parameters. First, β_i regulates a symptom's sensitivity to external triggers, with lower values reducing its likelihood of activation. Second, α , the elements of the weight matrix A , include α_{ii} , representing a self-reinforcing loop for symptom S_i , and α_{ji} , capturing the influence of symptom S_j on S_i . Third, δ_i introduces nonlinear amplification, where the influence of connected symptoms increases as S_i becomes more active. The stochastic term $\sigma_i dW_i$ represents independent additive noise for each symptom, where W_i is a standard Wiener process. In discrete time, this means that at each time step we add a Gaussian perturbation with mean 0 and variance dt , scaled by the symptom-specific noise amplitude σ_i . Formally, the Wiener increment satisfies $\Delta W_i(t) \sim \mathcal{N}(0, dt)$; equivalently, $\Delta W_i(t) = \sqrt{dt} \varepsilon_i(t)$ with $\varepsilon_i(t) \stackrel{\text{i.i.d.}}{\sim} \mathcal{N}(0, 1)$. Thus, the stochastic increment in the Euler-Maruyama update is implemented as $\Delta \sigma_i W_i(t) = \sigma_i \sqrt{dt} \varepsilon_i(t)$. For a comprehensive description of the model and its stochastic formulation, see Park, Waldorp, and Vasconcelos [16].

Numerical implementation and boundary handling. We simulate Eq. 1 using an Euler-Maruyama discretization with time step dt ($dt = 0.1$; see Table 1). Let $f_i(\mathbf{S}(t))$ denote the drift term in Equation 1. At each step,

$$S_i(t + dt) = S_i(t) + f_i(\mathbf{S}(t)) dt + \sigma_i \sqrt{dt} \varepsilon_i(t), \quad (2)$$

FEEDBACK LOOPS IN SYMPTOM NETWORKS

where $\varepsilon_i(t) \stackrel{\text{i.i.d.}}{\sim} \mathcal{N}(0, 1)$ are independent across symptoms and time steps. Because stochastic increments can temporarily move S_i outside the admissible interval $[0, 1]$, we enforce bounded symptom levels via reflection at the boundaries (no-flux conditions): values above 1 or below 0 are folded back into $[0, 1]$ (e.g., $1.3 \mapsto 0.7$, $-0.2 \mapsto 0.2$), consistent with the reflected diffusion formulation described in Park, Waldorp, and Vasconcelos [16] (see Appendix on reflective boundaries; see also [58, 59]).

Generating Synthetic Network Configurations

Given the reference network shown in Figure 1, we explore all possible network configurations by systematically altering the direction of the edges. The total number of possible synthetic network configurations is 2^n , where n is the number of *independent* edges—by *independent*, we mean that changing the direction of one edge does not affect the ability to change the direction of another, allowing for the creation of unique configurations. In our reference network, there are 17 edges in total, but two of these — forming a feedback loop between *sad* and *guilt* — are *dependent*, meaning the loop remains unchanged if both edges are flipped simultaneously. This reduces the number of independent edges to 15. The feedback loop itself can have 3 distinct configurations: (1) both edges in their original direction, maintaining the loop, (2) one edge flipped while the other remains unchanged, causing both edges to point in the same direction, or (3) the other edge flipped, reversing the direction. Instead of the 4 possible combinations (2^2), this loop yields only 3 unique configurations. The remaining 15 independent edges can produce 2^{15} possible configurations. Combining these with the 3 unique configurations of the feedback loop, the total number of unique network configurations derivable from our reference network is $2^{15} \times 3 = 98,304$. When generating directed configurations, we preserve the corresponding weight magnitudes from the reference matrix and only change edge direction; consequently, all nonzero weights remain positive, and no rescaling or normalization is applied after orientation. Once all synthetic network configurations are generated, the algorithm identifies feedback loops within each network using a *depth-first search* (DFS) algorithm [60]. This

FEEDBACK LOOPS IN SYMPTOM NETWORKS

algorithm systematically traverses the graph, detecting feedback loops by checking if a node is revisited within the same path, which indicates the presence of a loop. The process continues recursively, exploring all possible paths within the network.

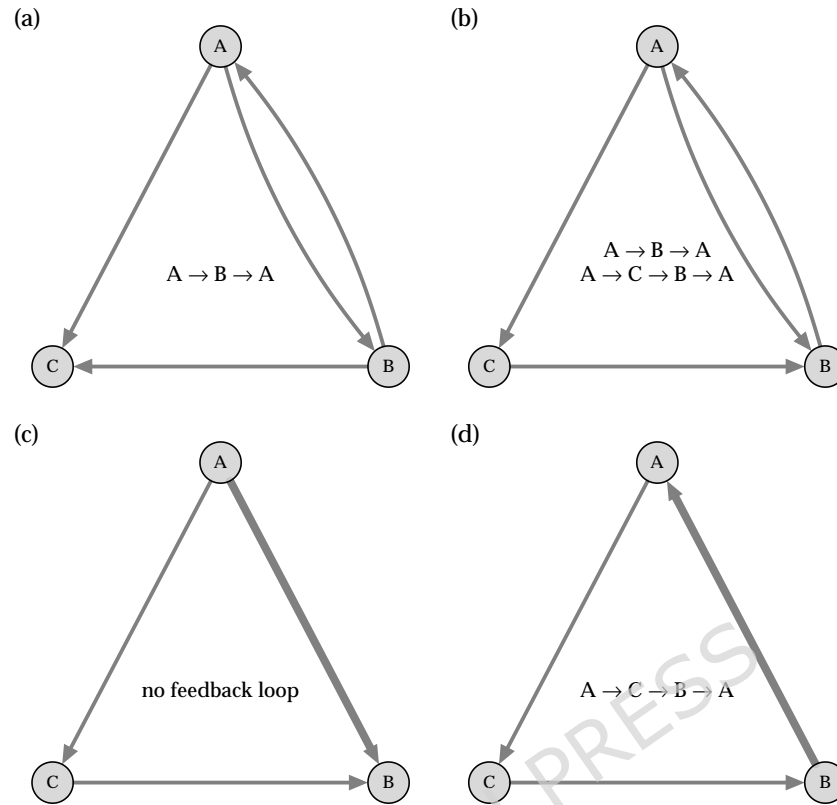
Figure 9 demonstrates the algorithm in action, using the network shown in Figure 9(a) as an example. The algorithm begins by generating all possible network configurations. In this case, there are two independent edges and two dependent edges involved in a feedback loop between nodes *A* and *B*. By altering the direction of each edge, the algorithm produces $2^2 \times 3 = 12$ synthetic network configurations. Figures 9(b), (c), and (d) illustrate three examples of these configurations. Once the synthetic network configurations are generated, the algorithm converts the matrix representation of each graph into an adjacency list, which contains the connections of each node to the other nodes in the network. The DFS algorithm then uses this adjacency list to explore the graph. Starting from each node, the algorithm follows the list to explore all possible paths. If a node is revisited along the same path, it indicates the presence of a feedback loop. These loops, along with their specific paths, are then recorded, as shown in Figure 9. For a detailed description of the algorithm used to generate all feasible synthetic network configurations and detect feedback loops, please refer to Appendix A.

Topological Features

In this section, we examine several key topological features to understand how the structure of feedback loops impacts symptom persistence. These features include the total number of feedback loops, the degree of overlap between these loops, the variability in weighted degrees, and frequency of nodes and edges involved in feedback loops. Throughout, “feedback loops” refer to directed cycles involving ≥ 2 distinct symptoms. Diagonal self-effects (α_{ii}) are treated as intrinsic symptom persistence in the underlying dynamics and are excluded from loop counts and other measures.

We hypothesize that the number of feedback loops will be positively correlated with symptom persistence, meaning the more cycles there are, the longer the symptoms are likely to

FEEDBACK LOOPS IN SYMPTOM NETWORKS

**Figure 9**

Example networks illustrating the steps of the algorithm for generating all feasible synthetic network configurations and detecting feedback loops in each network.

persist. Feedback loops represent cycles of symptoms reinforcing each other, and the more cycles present, the stronger and more sustained this reinforcement can be, leading to prolonged symptoms. However, this relationship is not straightforward. It is important to nuance this hypothesis by considering that some loops may overlap. For a given number of cycles, overlap between them may reduce their collective impact. When feedback loops overlap, their influence on the network becomes less distinct because shared nodes and edges create interdependencies, causing these loops to function more like a single cycle rather than separate, independent ones. This interconnection suggests that while the number of cycles increases, the actual impact of each cycle may be diluted.

To better understand how these loops interact, we measure the degree of overlap between

FEEDBACK LOOPS IN SYMPTOM NETWORKS

them. Greater overlap indicates that the loops are increasingly dependent on shared nodes and edges. As the degree of overlap increases, these feedback loops begin to operate as a single, more unified loop, reducing their individual impact. Therefore, analyzing the overlap allows us to distinguish between independent and interdependent feedback loops, providing a more nuanced understanding of the network's dynamics and its effect on symptom progression.

In addition to the number of cycles and their overlap, we also examine the variability in weighted degrees across the network. This measure helps us understand how the connectivity is distributed among the symptom nodes. A network with low variability indicates that activation is evenly spread across symptoms, allowing for a more balanced influence between them. In contrast, a network with high variability suggests that some symptoms have greater influence over others, possibly leading to more localized activations. By examining connectivity variability, we can understand how the influence of specific symptoms propagates through the network. This measure complements our analysis of feedback loop structures by providing a broader perspective on the overall configuration of the network and the centrality of particular symptoms.

Lastly, we examine node- and edge-level participation in feedback loops to identify structural patterns that significantly influence symptom dynamics. By measuring how frequently each node and edge appears in these loops, we can assess their relative influence on symptom persistence. Nodes and edges with higher recurrence are likely to play a more central role in driving symptom dynamics. Identifying these critical components helps us better understand the structural elements of feedback loops that contribute to symptom reinforcement within the system.

Feedback Loop and Overlap Level

We assess the total number of feedback loops by counting the unique loops detected by the algorithm described above. To evaluate the amount of overlap among these loops, we analyze node frequencies within the feedback loops. Let $C_i = \{c_1^{(i)}, c_2^{(i)}, \dots, c_{n_i}^{(i)}\}$ denote the set of all feedback loops in network i (of the 98,304 networks), where $c_k^{(i)}$ represents the k -th loop in network i and $n_i = |C_i|$ is the total number of loops of network i . For each node $v_j \in V_i$, where

FEEDBACK LOOPS IN SYMPTOM NETWORKS

$V_i = \{v_1, v_2, \dots, v_9\}$ represents the set of 9 nodes in network i , the frequency $f_{v_j,i}$ of node v_j appearing in any feedback loop is defined as:

$$f_{v_j,i} = \sum_{k=1}^{n_i} \mathbf{1}_{v_j \in c_k^{(i)}},$$

where $\mathbf{1}_{v_j \in c_k}$ is an indicator function that equals 1 if node v_j is part of loop c_k , and 0 otherwise.

When assessing the degree of overlap among feedback loops, we square the frequencies $f_{v_j,i}$ to emphasize the influence of nodes that participate in multiple loops. These nodes have a disproportionately stronger effect on the network dynamics due to the interdependencies of overlapping loops. The overlap level is then calculated by normalizing the squared frequencies by the square of the total number of loops:

$$O_i = \frac{\sum_{j=1}^9 f_{v_j,i}^2}{n_{c,i}^2}$$

Intuitively, O_i is low when loops are largely disjoint (few shared nodes) and increases as more loops share the same nodes, indicating that feedback becomes concentrated on a subset of symptoms. This nonlinear scaling highlights the stronger influence of nodes involved in overlapping loops, as their impact on the network dynamics tends to compound. Treating loop participation linearly would underestimate the significance of such interdependent connections, potentially obscuring critical patterns in feedback interactions. The overlap level is set to 0 when the number of feedback loops is fewer than 2 ($n_{c,i} < 2$), avoiding undefined or insignificant values.

Weighted Degree Variability

Finally, we calculate the weighted degree variability of each network to understand the distribution of connectivity. We define the weighted degree variability for network i as the sum of the standard deviations for the incoming and outgoing weighted degrees:

$$\text{weighted degree variability } (\sigma_{tot,i}) = \sigma_{in,i} + \sigma_{out,i},$$

FEEDBACK LOOPS IN SYMPTOM NETWORKS

where $\sigma_{in,i} = \text{sd} \left(\{d_{v_j,i}^{in}\}_{v_j \in V_i} \right)$ and $\sigma_{out,i} = \text{sd} \left(\{d_{v_j,i}^{out}\}_{v_j \in V_i} \right)$. Here, $\{d_{v_j,i}^{in}\}_{v_j \in V_i}$ and $\{d_{v_j,i}^{out}\}_{v_j \in V_i}$ represent the sets of incoming and outgoing weighted degrees for nodes v_j in network i , respectively. This measure provides insight into the distribution of connectivity across the network. Lower variability indicates a more uniform activation of symptoms across the network, whereas higher variability suggests that certain symptoms dominate the network's dynamics, leading to more localized patterns of activation.

Node and Edge Frequencies in Feedback Loops

To quantify the frequency of nodes and edges involved in feedback loops, we determine their frequency by counting their occurrences across the feedback loops in the network. For each node $v_j \in V_i$ in network i , the frequency $f_{v_j,i}$ of node v_j appearing in any feedback loop is:

$$f_{v_j,i} = \sum_{k=1}^{n_i} \mathbf{1}_{v_j \in c_k^{(i)}},$$

Similarly, the edge frequency $f_{e,i}$ for an edge e in network i is determined by the number of times this edge appears in any feedback loop across the n_i loops:

$$f_{e,i} = \sum_{k=1}^{n_i} \mathbf{1}_{e \in c_k^{(i)}}$$

For both node and edge frequencies, we normalize them by dividing by the total frequency across all nodes or edges in the network:

$$f_{v_j,i}^{\text{norm}} = \frac{f_{v_j,i}}{\sum_{j=1}^V f_{v_j,i}} \quad \text{and} \quad f_{e,i}^{\text{norm}} = \frac{f_{e,i}}{\sum_{e \in E_i} f_{e,i}},$$

where the sums are taken over all nodes $v_j \in V_i$ and all edges $e \in E_i$ in network i .

These frequencies quantify the relative importance of each node and edge in the feedback loop dynamics of the network. By analyzing these frequencies, we can identify which nodes and edges are central to the feedback loop structure and their role in symptom dynamics.

Together, these topological features help us understand how symptom persistence unfolds

FEEDBACK LOOPS IN SYMPTOM NETWORKS

in the network. By examining the number of feedback loops, their overlap, variability in connectivity, and the role of individual nodes and edges, we can see how different structural patterns influence symptom dynamics. In particular, identifying nodes and edges that appear more frequently in feedback loops helps highlight which symptoms and connections may have a stronger impact on persistence. Analyzing these features gives us a clearer picture of how symptom interactions contribute to the maintenance of mental health conditions.

Simulation Setup

We simulate symptom dynamics over time using the previously described SDEs in Eq.1, examining each synthetic network configuration to assess the impact of network structure — particularly topological features associated with feedback loops — on the progression of depression symptoms. Each simulation tracks the dynamics of nine symptoms over 2000 time units (t). We introduce a transient external shock starting at $t = 50$ and lasting for 300 time units ($50 \leq t \leq 350$), intended to represent an acute stressor (e.g., a major adverse life event). The shock is implemented by temporarily increasing each symptom's sensitivity parameter β_i from its baseline value $\beta^{original}$ to a less negative value β^{shock} (Table 1). Intuitively, β_i controls a symptom's baseline susceptibility to activation: in the baseline regime $\beta_i < 0$, and shifting β_i closer to zero reduces resistance to activation and biases the dynamics toward higher symptom levels. After the shock window ($t > 350$), β_i returns to its baseline value, and all other parameters (interaction weights α , nonlinear amplification δ , and noise parameters) are held fixed throughout. For an illustration of how changing β_i shifts the system between dynamical regimes, see the bifurcation diagram as a function of β_i in Park, Waldorp, and Vasconcelos [16, Fig. 2].

Detailed parameter values are summarized in Table 1. These values ensure bistability for each symptom in the original reference network [16]. In our analyses, this condition is not enforced for every directed configuration, because we systematically vary edge directions to explore a broad range of feedback-loop architectures.

Due to the stochastic nature of the SDE, each network configuration is simulated 50 times,

FEEDBACK LOOPS IN SYMPTOM NETWORKS

yielding 4,915,200 simulations in total ($50 \times 98,304$ configurations). For each run, we aggregate symptom levels across all nine symptoms and record the aggregated level at five post-shock time points: $t = 400, 800, 1200, 1600,$ and 2000 .

Table 1

Overview of Parameter Values Used in the Simulation.

Parameter	Description	Values
α	Elements of the weighted adjacency matrix A .	See matrix A .
$\beta^{original}$	Sensitivity levels of symptoms to external perturbations during the normal period.	$\beta^{original} = [-1.01, -0.52, -0.53, -1.01, -0.82, -0.52, -0.75, -1.10, -0.80]$.
β^{shock}	Sensitivity levels of symptoms to external perturbations during the shock period.	$\beta^{shock} = [-0.67, -0.34, -0.35, -0.67, -0.54, -0.34, -0.50, -0.74, -0.54]$.
S_0	Initial values of symptom intensities.	$S_{i_0} = 0.01, \forall i = 1, \dots, 9$.
δ	Boosting factor that amplifies the effects of other symptoms S_j on symptom S_i .	$\delta_i = 9, \forall i = 1, \dots, 9$.
σ	Scaling factor controlling the strength of the stochastic term.	$\sigma_i = 0.14, \forall i = 1, \dots, 9$.
dt	Time step for updating the symptom intensities.	$dt = 0.1$.

In this section, we perform an empirical analysis using time series data from clinical patients to assess external consistency between the simulation-derived patterns and networks estimated from patient data. To do this, we apply a causal discovery algorithm to estimate directed causal networks from the clinical data. By analyzing the frequency of directed edges in these networks, we compare the patterns observed in the individual patient data with those derived from our simulations. This comparison helps us assess the ability and robustness of our simulation models in capturing the dynamics of real-world symptom interactions. In the following, we briefly introduce the dataset and the causal discovery algorithm used, and present the results of this empirical analysis.

Empirical dataset and causal discovery

Data. We analyze data from a randomized clinical trial on chronic depression conducted in eight clinical sites in Germany [24]. The trial included 254 patients who were randomly assigned to receive 32 sessions of disorder-specific or nonspecific psychotherapy for 48 weeks.

FEEDBACK LOOPS IN SYMPTOM NETWORKS

During each session, participants assessed their depressive symptoms, which included the nine major symptoms of depressive disorder defined by the DSM-5, before and after the session [61]. Symptom scores were dichotomized as "0: symptom not present" and "1: symptom present" [42]. For our analysis, we utilize all the available pre-session data to capture symptom dynamics over time.

Causal discovery. To analyze the time-series symptom data, we employ the PCMCI+ algorithm (PC Momentary Conditional Independence), a causal discovery method specifically designed for time-series data [22]. PCMCI+ is capable of identifying both lagged ($\tau > 0$) and contemporaneous ($\tau = 0$) causal relationships, disentangling temporal and simultaneous influences.

Based on the foundations of the PC algorithm [62], the PCMCI+ algorithm relies on several key assumptions that are central to most causal discovery methods. First, PCMCI+ relies on the *causal Markov* assumption, which states that each variable is independent of its non-descendants, given its parents in the causal graph. It also assumes the *faithfulness assumption*, meaning that any conditional independence relations in the data are reflective of the causal structure. These assumptions are fundamental for identifying valid causal links in the data. Additionally, PCMCI+ assumes *causal sufficiency*, meaning that there are no hidden confounders affecting the relationships between variables. Finally, when identifying time-lagged causal relationships, PCMCI+ assumes that the causal links are *stationary*. This means that if a causal relationship $X_{t-\tau} \rightarrow X_t$ holds at a given time t , then the same relationship $X_{t'-\tau} \rightarrow X_{t'}$ holds at all other time points $t' \neq t$. Together, these assumptions allow PCMCI+ to effectively uncover both contemporaneous and time-lagged causal relationships in time-series data while accounting for potential confounding and spurious correlations. These assumptions, especially causal sufficiency and faithfulness, may not be fully met in psychological data where unmeasured confounding and overlapping causal processes are common. We therefore interpret the estimated causal graphs cautiously and as preliminary.

The PCMCI+ algorithm operates in two distinct phases: the *lagged skeleton phase*, which

FEEDBACK LOOPS IN SYMPTOM NETWORKS

identifies causal links over time lags ($X_i^{t-\tau} \rightarrow X_j^t$), and the *contemporaneous skeleton phase*, which detects direct same-time causal relationships ($X_i^t \rightarrow X_j^t$) and refines these relationships to account for confounding from shared lagged causes. The final causal graph distinguishes between lagged causal links, which are represented as curved arrows, and contemporaneous causal links, which are depicted as straight arrows. Because the contemporaneous phase relies on a PC-type procedure, the contemporaneous structure is identifiable only up to a *Markov equivalence class*—a set of graphs that encode the same conditional (in)dependencies (i.e., satisfy the same d-separation relations) [63]. Accordingly, the contemporaneous component is represented as a *completed partially directed acyclic graph* (CPDAG), where some adjacencies may remain unoriented when multiple directions are compatible with the data; these are denoted by straight lines with circle ends ($X_i^t \circ \rightarrow X_j^t$). Following the PC-MCI+ literature, the combined output is sometimes referred to as a *time-series CPDAG* [22]. In this analysis, we set the maximum time delay (τ_{max}) to 3 and the significance level (α_{PC}) to 0.01, using the G-squared conditional independence test to accommodate the binary nature of the dataset. For more details on the PC-MCI+ algorithm, we refer readers to [22].

Data and Code Availability

The code and data for this study are publicly available on GitHub at: <https://github.com/KyuriP/RoleFeedack>. The core workflow for generating directed configurations and quantifying feedback-loop architecture is also available as an accompanying R package, `causalnet` (CRAN), which includes a vignette illustrating the main pipeline; a more extensive tutorial paper is in preparation. Detailed instructions on how to reproduce the analyses presented in this paper can be found in the repository. Data were analyzed using R version 4.4.1 [64] and Python version 3.12.2. All relevant packages and their dependencies are also listed in the repository. Due to the computational demands of large-scale simulations, analyses were conducted on the *Snellius* supercomputer (*genoa* partition, 192-core nodes). Please note that the study’s design and analysis were not pre-registered.

FEEDBACK LOOPS IN SYMPTOM NETWORKS

Funding

This work was supported by ZonMW under the project “How can we best act upon contextual factors that influence mental health in lower socio-economic groups? Insights offered by system dynamics methodologies” (dossier number: 05550032110014). KP and VVV acknowledge this funding support.

ARTICLE IN PRESS

References

- [1] Denny Borsboom and Angélique O.J. Cramer. “Network Analysis: An Integrative Approach to the Structure of Psychopathology.” In: *Annual Review of Clinical Psychology* 9.1 (2013), pp. 91–121. doi: [10.1146/annurev-clinpsy-050212-185608](https://doi.org/10.1146/annurev-clinpsy-050212-185608).
- [2] Alba Contreras et al. “The study of psychopathology from the network analysis perspective: A systematic review.” In: *Psychotherapy and psychosomatics* 88.2 (2019), pp. 71–83.
- [3] Donald J Robinaugh et al. “The network approach to psychopathology: A review of the literature 2008–2018 and an agenda for future research.” In: *Psychological medicine* 50.3 (2020), pp. 353–366.
- [4] Denny Borsboom et al. “Network analysis of multivariate data in psychological science.” en. In: *Nature Reviews Methods Primers* 1.1 (2021), pp. 1–18. issn: 2662-8449. doi: [10.1038/s43586-021-00055-w](https://doi.org/10.1038/s43586-021-00055-w). (Visited on 12/09/2022).
- [5] Eiko I Fried et al. “Mental disorders as networks of problems: a review of recent insights.” In: *Social psychiatry and psychiatric epidemiology* 52 (2017), pp. 1–10.
- [6] Payton J Jones and Donald Robinaugh. “So What? Implications of Network Theory for Research and Practice.” In: (2021).
- [7] Richard J. McNally. “Network Analysis of Psychopathology: Controversies and Challenges.” In: *Annual Review of Clinical Psychology* 17. Volume 17, 2021 (2021), pp. 31–53. issn: 1548-5951. doi: <https://doi.org/10.1146/annurev-clinpsy-081219-092850>.
- [8] Marieke Wichers. “The dynamic nature of depression: a new micro-level perspective of mental disorder that meets current challenges.” In: *Psychological medicine* 44.7 (2014), pp. 1349–1360.

FEEDBACK LOOPS IN SYMPTOM NETWORKS

- [9] Denny Borsboom. “A network theory of mental disorders.” en. In: *World Psychiatry* 16.1 (2017), pp. 5–13. ISSN: 2051-5545. DOI: [10.1002/wps.20375](https://doi.org/10.1002/wps.20375).
- [10] Philip W Gold. “The organization of the stress system and its dysregulation in depressive illness.” In: *Molecular psychiatry* 20.1 (2015), pp. 32–47.
- [11] Angélique O. J. Cramer et al. “Comorbidity: A network perspective.” In: *Behavioral and Brain Sciences* 33.2–3 (2010), pp. 137–150. DOI: [10.1017/S0140525X09991567](https://doi.org/10.1017/S0140525X09991567).
- [12] Jeroen F Uleman et al. “Mapping complex public health problems with causal loop diagrams.” In: *International Journal of Epidemiology* 53.4 (2024).
- [13] Jonas Haslbeck et al. “Modeling psychopathology: From data models to formal theories.” In: *Psychological Methods* 27.6 (2022), p. 930.
- [14] Peder M Isager. “On the role of causal direction and feedback in network theories of mental disorder.” In: (2023).
- [15] Gabriela Lunansky et al. “Bouncing back from life’s perturbations: Formalizing psychological resilience from a complex systems perspective.” In: *Psychological Review* (2024).
- [16] Kyuri Park, Lourens Waldorp, and Vítor Vasconcelos. *The Individual- and Population-level Mechanistic Implications of Statistical Networks of Symptoms*. Jan. 19, 2025. DOI: [10.31234/osf.io/ysqtr](https://doi.org/10.31234/osf.io/ysqtr). URL: <https://osf.io/ysqtr> (visited on 01/20/2025).
- [17] Zhi Jing et al. “Comparing Depression Prevalence and Associated Symptoms with Intolerance of Uncertainty among Chinese Urban and Rural Adolescents: A Network Analysis.” en. In: *Behavioral Sciences* 13.8 (Aug. 2023). Number: 8 Publisher: Multidisciplinary Digital Publishing Institute, p. 662. ISSN: 2076-328X. DOI: [10.3390/bs13080662](https://doi.org/10.3390/bs13080662). URL: <https://www.mdpi.com/2076-328X/13/8/662> (visited on 01/07/2024).

FEEDBACK LOOPS IN SYMPTOM NETWORKS

- [18] Eun-Hyun Lee et al. “Measurement invariance of the patient health questionnaire-9 depression scale in a nationally representative population-based sample.” In: *Frontiers in Psychology* 14 (2023). ISSN: 1664-1078. URL: <https://www.frontiersin.org/articles/10.3389/fpsyg.2023.1217038> (visited on 01/07/2024).
- [19] Cristian Ramos-Vera, Jonatan Banos-Chaparro, and Roseline Oluwaseun Ogundokun. *The network structure of depressive symptomatology in Peruvian adults with arterial hypertension*. en. Tech. rep. 10:19. Type: article. F1000Research, Mar. 2021. DOI: [10.12688/f1000research.27422.2](https://doi.org/10.12688/f1000research.27422.2). URL: <https://f1000research.com/articles/10-19> (visited on 01/07/2024).
- [20] Sacha Epskamp et al. “The Gaussian graphical model in cross-sectional and time-series data.” In: *Multivariate behavioral research* 53.4 (2018), pp. 453–480.
- [21] Oisín Ryan, Laura F Bringmann, and Noémi K Schuurman. “The challenge of generating causal hypotheses using network models.” In: *Structural Equation Modeling: A Multidisciplinary Journal* 29.6 (2022), pp. 953–970.
- [22] Jakob Runge. “Discovering contemporaneous and lagged causal relations in autocorrelated nonlinear time series datasets.” In: *Conference on Uncertainty in Artificial Intelligence*. Pmlr. 2020, pp. 1388–1397.
- [23] Jakob Runge et al. “Inferring causation from time series in Earth system sciences.” In: *Nature communications* 10.1 (2019), p. 2553.
- [24] Elisabeth Schramm et al. “Effect of disorder-specific vs nonspecific psychotherapy for chronic depression: a randomized clinical trial.” In: *JAMA psychiatry* 74.3 (2017), pp. 233–242.
- [25] Angélique OJ Cramer et al. “Major depression as a complex dynamic system.” In: *PloS one* 11.12 (2016), e0167490.

FEEDBACK LOOPS IN SYMPTOM NETWORKS

- [26] Claudia van Borkulo et al. “Association of symptom network structure with the course of depression.” In: *JAMA psychiatry* 72.12 (2015), pp. 1219–1226.
- [27] William G. Jacoby. “Loess:: a nonparametric, graphical tool for depicting relationships between variables.” In: *Electoral Studies* 19.4 (2000), pp. 577–613. ISSN: 0261-3794. DOI: [https://doi.org/10.1016/S0261-3794\(99\)00028-1](https://doi.org/10.1016/S0261-3794(99)00028-1). URL: <https://www.sciencedirect.com/science/article/pii/S0261379499000281>.
- [28] William S Cleveland, Eric Grosse, and William M Shyu. “Local regression models.” In: *Statistical models in S*. Routledge, 2017, pp. 309–376.
- [29] Robert L Thorndike. “Who belongs in the family?” In: *Psychometrika* 18.4 (1953), pp. 267–276.
- [30] Peter M Lewinsohn et al. “Major depression in community adolescents: age at onset, episode duration, and time to recurrence.” In: *Journal of the American Academy of Child & Adolescent Psychiatry* 33.6 (1994), pp. 809–818.
- [31] Christopher JL Murray et al. “The Global Burden of Disease 2000 project: aims, methods and data sources.” In: *Geneva: World Health Organization* 36 (2001), pp. 1–57.
- [32] Filip Spaniel et al. “Relapse in schizophrenia: definitively not a bolt from the blue.” In: *Neuroscience letters* 669 (2018), pp. 68–74.
- [33] Laura F Bringmann, Sabine Martino, and George Panagopoulos. “What do centrality measures measure in psychological networks?” In: *Journal of Abnormal Psychology* 128.8 (2019), pp. 892–903. doi: [10.1037/abn0000446](https://doi.org/10.1037/abn0000446).
- [34] Tobias R Spiller et al. “On the validity of the centrality hypothesis in cross-sectional between-subject networks of psychopathology.” In: *BMC medicine* 18 (2020), pp. 1–14.
- [35] Zachary P Neal and Jennifer Watling Neal. “Out of bounds? The boundary specification problem for centrality in psychological networks.” In: *Psychological Methods* 28.1 (2023), p. 179.

FEEDBACK LOOPS IN SYMPTOM NETWORKS

- [36] Susan Nolen-Hoeksema, Blair E Wisco, and Sonja Lyubomirsky. “Rethinking rumination.” In: *Perspectives on psychological science* 3.5 (2008), pp. 400–424.
- [37] Sangmoon Kim, Ryan Thibodeau, and Randall S Jorgensen. “Shame, guilt, and depressive symptoms: a meta-analytic review.” In: *Psychological bulletin* 137.1 (2011), p. 68.
- [38] Jutta Joormann and Ian H Gotlib. “Emotion regulation in depression: Relation to cognitive inhibition.” In: *Cognition and Emotion* 24.2 (2010), pp. 281–298.
- [39] Roland Zahn et al. “The role of self-blame and worthlessness in the psychopathology of major depressive disorder.” In: *Journal of affective disorders* 186 (2015), pp. 337–341.
- [40] Erdem Pulcu et al. “Increased amygdala response to shame in remitted major depressive disorder.” In: *PloS one* 9.1 (2014), e86900.
- [41] Sophie Green et al. “Guilt-selective functional disconnection of anterior temporal and subgenual cortices in major depressive disorder.” In: *Archives of General Psychiatry* 69.10 (2012), pp. 1014–1021.
- [42] Lea Schumacher et al. “Implications of the network theory for the treatment of mental disorders: A secondary analysis of a randomized clinical trial.” In: *Jama Psychiatry* 80.11 (2023), pp. 1160–1168.
- [43] Jonas Haslbeck, Oisín Ryan, and Fabian Dablander. “The sum of all fears: Comparing networks based on symptom sum-scores.” In: *Psychological Methods* 27.6 (2022), p. 1061.
- [44] Giovanni Briganti, Marco Scutari, and Richard J McNally. “A tutorial on bayesian networks for psychopathology researchers.” In: *Psychological methods* 28.4 (2023), p. 947.
- [45] Thomas Richardson. *Discovering cyclic causal structure*. Tech. rep. CMU-PHIL-68. Pittsburgh, Pennsylvania: Carnegie Mellon University, Department of Philosophy, Feb. 1996.
- [46] Peter Spirtes. “An anytime algorithm for causal inference.” In: *International Workshop on Artificial Intelligence and Statistics*. PMLR. 2001, pp. 278–285.

FEEDBACK LOOPS IN SYMPTOM NETWORKS

- [47] Eric V. Strobl. “A constraint-based algorithm for causal discovery with cycles, latent variables and selection bias.” In: *International Journal of Data Science and Analytics* 8.1 (2019), pp. 33–56. ISSN: 2364-4168. DOI: [10.1007/s41060-018-0158-2](https://doi.org/10.1007/s41060-018-0158-2).
- [48] Ana Rita Nogueira et al. “Methods and tools for causal discovery and causal inference.” In: *Wiley interdisciplinary reviews: data mining and knowledge discovery* 12.2 (2022), e1449.
- [49] Matteo Malgaroli, Adam Calderon, and George A Bonanno. “Networks of major depressive disorder: A systematic review.” In: *Clinical Psychology Review* 85 (2021), p. 102000.
- [50] Marieke Wichers et al. “A narrative review of network studies in depression: What different methodological approaches tell us about depression.” In: *Frontiers in psychiatry* 12 (2021), p. 719490.
- [51] Kyuri Park, Lourens J Waldorp, and Oisín Ryan. “Discovering cyclic causal models in psychological research.” In: *advances. in/psychology* 2 (2024), e72425.
- [52] Peter Spirtes. “Directed cyclic graphical representations of feedback models.” In: *Proceedings of the Eleventh conference on Uncertainty in artificial intelligence*. Morgan Kaufmann. 1995, pp. 491–498.
- [53] K Kroenke, RL Spitzer, and JBW Williams. “The patient health questionnaire (phq-9)–overview.” In: *J. Gen. Intern. Med* 16 (2001), pp. 606–616.
- [54] Stefan G Hofmann, Joshua Curtiss, and Richard J McNally. “A complex network perspective on clinical science.” In: *Perspectives on Psychological Science* 11.5 (2016), pp. 597–605.
- [55] Raffael Kalisch et al. “Deconstructing and reconstructing resilience: a dynamic network approach.” In: *Perspectives on Psychological Science* 14.5 (2019), pp. 765–777.
- [56] Merijn Mestdagh et al. “Sidelining the mean: The relative variability index as a generic mean-corrected variability measure for bounded variables.” In: *Psychological Methods* 23.4 (2018), p. 690.

FEEDBACK LOOPS IN SYMPTOM NETWORKS

- [57] Peter H Schönemann. “Some theory and results for metrics for bounded response scales.” In: *Journal of Mathematical Psychology* 27.3 (1983), pp. 311–324.
- [58] Hiroshi Tanaka. “Stochastic differential equations with reflecting boundary condition in convex regions.” In: *Stochastic Processes: Selected Papers of Hiroshi Tanaka* 9 (1979), p. 157.
- [59] J Michael Harrison and Martin I Reiman. “Reflected Brownian motion on an orthant.” In: *The Annals of Probability* 9.2 (1981), pp. 302–308.
- [60] Robert Tarjan. “Depth-first search and linear graph algorithms.” In: *SIAM journal on computing* 1.2 (1972), pp. 146–160.
- [61] American Psychiatric Association, D.S.M.T.F. and American Psychiatric Association, D.S. *Diagnostic and statistical manual of mental disorders: DSM-5*. Vol. 5. 5. American psychiatric association Washington, DC, 2013.
- [62] Peter Spirtes and Clark Glymour. “An algorithm for fast recovery of sparse causal graphs.” In: *Social science computer review* 9.1 (1991), pp. 62–72.
- [63] Peter Spirtes, Clark Glymour, and Richard Scheines. *Causation, prediction, and search*. MIT press, 2001.
- [64] R Core Team. *R: A Language and Environment for Statistical Computing*. R Foundation for Statistical Computing. Vienna, Austria, 2024. URL: <https://www.R-project.org/>.